Eur. Phys. J. C (2025) 85:565
https://doi.org/10.1140/epjc/s10052-025-14294-8

THE EUROPEAN PHYSICAL JOURNAL C

Regular Article - Theoretical Physics

Parameter constraints and cosmographic analysis of Barrow agegraphic and new Barrow agegraphic dark energy models

Anamika Kotal[1,a], **Sayani Maity**[2,b], **Ujjal Debnath**[1,c], **Anirudh Pradhan**[3,d]

[1] Department of Mathematics, Indian Institute of Engineering Science and Technology, Shibpur, Howrah 711 103, India
[2] Department of Mathematics, Sister Nivedita University, DG-1/2, Action Area 1, New Town, Kolkata 700 156, India
[3] Centre for Cosmology, Astrophysics and Space Science (CCASS), GLA University, Mathura 281406, India

Received: 3 January 2025 / Accepted: 3 May 2025

Abstract This research focuses on examining a non-flat Friedmann–Robertson–Walker (FRW) cosmological model of the universe incorporating both dark matter and dark energy. Two intriguing dark energy models, Barrow agegraphic dark energy (BADE) and new Barrow agegraphic dark energy (NBADE), which were introduced in accordance with the holographic principle incorporating Barrow entropy, have been selected to play the role of dark energy. Using datasets from cosmic chronometers and baryon acoustic oscillations, we utilized the Markov Chain Monte Carlo (MCMC) technique to constrain the parameters of our model. This enables us to make several possible comparisons between these novel models of dark energy and the ΛCDM models. Here, we explore cosmological parameters, including the equation of state(EoS) parameter, jerk parameter, deceleration parameter, and cosmological planes such as the $q-r$ plane, $\omega_d - \omega_d'$ for different values of the model parameters by considering both the presence and absence of mutual interactions of the dark sector of the universe. In addition, we examined the thermal stability and the Swampland criteria of our constructed models. Additionally, we analyze the energy conditions and find that NEC and DEC are fulfilled, but SEC is broken, indicating model stability and supporting the current acceleration of the universe. In order to give a more precise explanation of the origin of cosmic structures, we lastly conduct a linear perturbation analysis to examine the growth in matter density perturbations.

1 Introduction

The mystery of dark energy, the exotic aspect of the cosmos that drives cosmic acceleration, remains one of the most intriguing subjects in theoretical and experimental cosmology. The holographic dark energy (HDE) concept stands out as one of the most compelling dark energy model candidates proposed in the literature. The holographic principle is the origin of it that connects the ultraviolet cut-off, the largest distance at a cosmological scale, and the infrared cut-off of a quantum theory [1]. According to this principle, the universe horizon entropy is characterized by its two-dimensional bounding area, which resembles the Black hole entropy area law of Benkenstein–Hawking. The first HDE model was introduced with the Hubble horizon as IR cut-off but was unable to describe the era of cosmic acceleration [2,3]. To this end, physicists assumed different IR cut-off scales and horizon entropy that yield a series of different HDE models. HDE model can be considered to be an alternative dark energy model that presents a time-varying dynamic equation of state and is consistent with the quantum principle that obeys the Heisenberg type uncertainty principle. HDE models also gained considerable success in problems describing the inflationary era and bounce scenario. However, the HDE model suffers from casualty problem and circular reasoning problem. To resolve these issues, Cai in 2007 proposed an agegraphic dark energy (ADE) model by inserting the age of the universe as the IR cut-off as opposed to horizon distance [4]. The energy density of agegraphic dark energy (ADE) [5] is given by

$$\rho_d = \frac{3n^2 M_p^2}{T^2}, \tag{1}$$

where n is a dimensionless parameter introduced to account for uncertainties, including the number of quantum fields

[a] e-mail: kotalanamika31@gmail.com
[b] e-mail: sayani.office88@gmail.com (corresponding author)
[c] e-mail: ujjaldebnath@gmail.com
[d] e-mail: pradhan.anirudh@gmail.com

Published online: 23 May 2025

present in the universe, potential corrections due to curved spacetime, and other quantum gravitational effects. The fractional energy densities are defined as $\Omega_d = \frac{\rho_d}{3M_p^2 H^2} = \frac{n^2}{H^2 T^2}$ and $\Omega_m = 1 - \Omega_d$. Using the matter energy conservation equation, $\dot{\rho}_m + 3H\rho_m = 0$, the equation of motion for Ω_d is obtained as

$$\Omega_d' = \Omega_d(1-\Omega_d)\left(3 - \frac{2}{n}\sqrt{\Omega_d}\right), \tag{2}$$

where a prime denotes differentiation with respect to the e-folding time $N = \ln a$. The equation-of-state (EoS) parameter for ADE is given by

$$w_d = -1 + \frac{2}{3n}\sqrt{\Omega_d}, \tag{3}$$

which shows that at early times ($\Omega_d \to 0$), the dark energy behaves like a cosmological constant ($w_q \to -1$), while at late times ($\Omega_d \to 1$), it deviates slightly as $w_d \to -1 + \frac{2}{3n}$. However, a fundamental inconsistency arises in the matter-dominated epoch. While the evolution Eq. 2 suggests $\Omega_d \propto a^3$, the age of the universe scales as $T^2 \propto a^3$, leading to $\rho_d \propto a^{-3}$, which implies Ω_d remains constant, contradicting $\Omega_d \propto a^3$. Moreover, since ADE adapts to the universe's dominant component (matter or radiation), it never dominates, making it unable to drive late-time cosmic acceleration. This formulation depends on the cosmic age T, which varies significantly across different epochs. As a result, ADE does not provide a universal framework that is valid from the early universe to the present. Instead, its behavior is strongly epoch-dependent: in the early universe, it mimics a cosmological constant but does not dominate; in the matter-dominated era, its scaling behavior introduces inconsistencies that prevent it from naturally overtaking matter; and only at late times does it become significant. This reliance on cosmic age makes ADE fundamentally different from ΛCDM and quintessence, which remain valid in all cosmic epochs. Reference [6] use observational data for a high-redshift quasar (APM 08279+5255 with $z = 3.91$) and two old galaxies (LBDS 53W091 with $z = 1.55$ and LBDS 53W069 with $z = 1.43$) to examine the age constraint imposed by the agegraphic dark energy (ADE) model. While the ADE model easily accommodates the galaxies, a lower Hubble parameter ($h = 0.64$) is needed to fit the quasar data, assuming $\Omega_{m0} \approx 0.22$. The age crisis persists until the present Hubble parameter is less than the WMAP3 optimal fit, such as $h = 0.59$, suggested by Sandage and collaborators. However, if it is assumed that the dark energy model's specific numerical parameter is of order one, then this dark energy is consistent with astronomical data. Early on, the dark energy acts as a cosmological constant, and later on, it propels the cosmos toward an infinitely faster expansion with a power-law shape. Several modifications have been proposed to resolve this issue, including the new agegraphic dark energy (NADE) model, which replaces the cosmic age with conformal time, interacting ADE models that allow energy transfer between matter and dark energy, and generalized ADE models that introduce dynamical corrections to ensure the proper transition to dark energy domination. Despite these limitations, ADE provides a phenomenologically interesting framework for researching the universe's dark energy evolution. Although the ADE model can explain the accelerated expansion of the universe and is able to avoid the casualty problem, it is unable to demonstrate the matter-dominated era and imitate the late-time cosmological constant. In this regard, the energy density of the ADE model was modified by taking the time scale as conformal time, the model named as new agegraphic dark energy (NADE) model [7]. While the agegraphic dark energy (ADE) model lacks universality due to its direct dependence on the age of the Universe, the new agegraphic dark energy (NADE) model is formulated in terms of conformal time, which provides a more generalized framework. However, the NADE model still faces certain limitations tied to specific cosmological epochs. In particular, it has been shown that NADE can only correctly depict the far-past matter (radiation)-dominated era when the parameter n is selected to be greater than a critical value n_c, numerically determined as $n_c = 2.6878$ (during the matter-dominated phase) and $n_c = 2.513775$ (during the radiation-dominated phase) [8]. The NADE model struggles to accommodate the old quasar APM 08279+5255 ($z = 3.91$), known as the "age problem," while remaining consistent with cosmological observations. Introducing an interaction between dark energy and dark matter in the framework of the interacting new agegraphic dark energy (INADE) model resolves this issue, successfully fitting the quasar's age at the 2σ level under current constraints without significantly altering other cosmological parameters [9]. In practice, NADE functions as a single-parameter model, as opposed to the two-parameter ADE model [10], because of its unique analytical properties during the epochs dominated by radiation and matter. All of NADE's other physical quantities are calculated in accordance with the single model parameter n. As long as n is of order unity, this work suggests that the coincidence problem can be inherently addressed in the NADE model [11]. Later on, various ADE models were proposed in the literature, such as the Tsallis agegraphic dark energy (TADE) model [12], the new Tsallis agegraphic dark energy (NTADE) model [13], by choosing various entropy formalisms.

Recently, inspired by the quantum fluctuation effects, Barrow made the manifestation of the quantum gravitational process, leading to complex fractal patterns in the structure of a black hole. This complex structure yields a finite volume but with infinite or finite area, indicating the requirement of modification of the BH entropy as [14,15]

$$S_{BH} = \left(\frac{A}{A_0}\right)^{1+\frac{\Delta}{2}}, \tag{4}$$

where A, A_0, and Δ are the horizon area, Plank area, and parameter to specify the quantum gravitational deformation effect in Barrow entropy, respectively. Δ ranges over [0, 1]. For $\Delta = 0$, the Benkenstein–Hawking entropy is restored, and $\Delta = 1$ yields maximum deformation and the horizon's fractal structure. E. N. Saridakis inserted the Barrow entropy into the Holographic dark energy model and introduced the Barrow Holographic dark energy framework (BHDE) given by

$$\rho_{BHDE} = CL^{\Delta-2}, \quad \text{where } C = 3c^2M_P^2. \tag{5}$$

M_P, c^2, L, and Δ, are the Planck mass, the model parameter, the infrared (IR) cut-off length, and the parameter that measures the effects of quantum gravitational deformation, respectively. By using Barrow entropy instead of the standard Bekenstein–Hawking entropy and starting with the conventional holographic principle, the Barrow holographic dark energy (BHDE) offers an intriguing substitute for the quantitative explanation of dark energy [16]. In the limit where the Barrow entropy [17] reduces to the standard Bekenstein–Hawking entropy, Saridakis [18] has shown that BHDE can incorporate basic holographic dark energy (HDE) as a special case [19,20]. The quantum-gravitational correction to the horizon could provide a more accurate representation of nature, potentially addressing long-standing cosmological questions. It is important to note that BHDE is not derived from specific quantum gravity calculations but rather from general physical principles; however, it bears similarities to Tsallis nonextensive entropy [21–23]. The author has also shown that the Barrow holographic dark energy model can accurately describe the thermal evolution of the universe, including the transition from the matter-dominated era to the dark energy era. This framework presents a novel context with rich and intriguing phenomenology.He has further investigated a cosmological scenario using gravity-thermodynamics conjecture with Barrow-entropy that yields modified Friedmann equations with the appearance of a new extra term constituting the effective energy density. It was found that these new additional terms vanish if the Barrow entropy is reduced to the standard Bekenstein–Hawking one [24].

The study in reference [25] explores the inflationary mechanism controlled by BHDE (Barrow holographic dark energy). Various aspects of BHDE models have been studied largely in the literature, for example, [26–28]. Next, the Barrow agegraphic dark energy (BADE) model was introduced in reference [29], utilizing the age of the universe and conformal time as the infrared cut-off, where it was observed that the BADE model exhibits a stable nature in the past. In [27], the statefinder parameters of the BADE model in (r, s) and (r, q) planes have been investigated and observed that for a range of model parameter value Δ, the model behaves like Chaplygin gas and quintessence. In ref [29], the new Barrow agegraphic dark energy (NBADE) model was introduced by inserting the conformal time as the IR cutoff. In Ref. [30], the phase space analysis of the BADE model has been conducted, and the model is found to mimic the behavior of a cosmological constant. In Ref. [31], the new Barrow agegraphic dark energy (NBADE) model has been analyzed by choosing the distinct values of the Barrow model parameter δ in the background of Friedmann–Robertson–Walker (FRW) Universe. In a non-flat cosmos, the thermal stability and cosmic dynamics of Barrow holographic dark energy have been explored in [32]. Motivated by these works, in this study, we focus on two distinct dark energy models: the Barrow agegraphic dark energy (BADE) model and the new Barrow agegraphic dark energy (NBADE) model. For each model, we examine two scenarios: the interacting scenario (denoted as BADEI and NBADEI for BADE and NBADE, respectively), where dark energy interacts exclusively with dark matter, and the non-interacting scenario, where no such interaction is considered, in the non-flat FRW universe.

Modern cosmology is based on the fundamental principle of constraining the parameters of the cosmological model, including the Hubble constant, curvature, and density parameters, using data. By comparing theoretical predictions or expressions for observables with observations, cosmologists use this method to estimate values of model parameters. They then adjusted the model parameters until the theoretical prediction and observations coincided as much as possible. To constrain BADE and NBADE and notably to establish observable limits on the novel Barrow coefficient that measures the modification due to quantum gravitational effects and, as a result, the departure from the standard holographic dark energy, we aim to use observational data from baryon acoustic oscillation (BAO) observations and direct observations of the Hubble constant using cosmic chronometers (CC). For the purpose of accomplishing this, we used the covariance matrix technique, which allowed us to identify the ideal values for a number of crucial parameters in our suggested model and minimize the related errors. In this regard, we should draw attention to some of the pioneering data analysis research projects conducted in the literature. In Reference [33], the authors studied the BHDE model in a non-flat FRW universe, incorporating supernova type Ia observations and Hubble data, and showed that it is capable of explaining the universe's thermal history. In Reference, the authors [34] analyzed the TADE and NTADE models in a flat Friedmann–Robertson–Walker (FRW) spacetime, focusing on the equation of state(EoS) and deceleration parameters. Recently, Mahmoudifard et al. [35] analyzed the BHDE model in an FRW universe, incorporating relic neutrinos to constrain parameters (α, β), the total neutrino

mass m_v, and the viable number of species N_{eff} using the latest observational data. By establishing a correspondence between Einstein-ther gravity and the BADE and NBADE models, the authors were able to constrain the parameters using observational data and obtain important insights [36]. For other works on observational constraints, see References [31,37–40]. In [41] the inflationary regime of the Universe has been investigated in the context of a modified cosmological scenario based on the gravity-thermodynamics conjecture with Barrow entropy. The effect of the chosen entropy on the inflationary dynamics has been explored with a power-law behavior of the scalar inflation field. In [42], the interaction between non-extensive entropic FLRW cosmology and the power-law inflationary model has been examined. It has been observed that the effect of entropies like Tsallis, Rényi, and Sharma-Mittal entropies, uncover a significant correlation with the power-law inflationary dynamics.

Deeper understanding of dark energy and its impact on cosmic development has been demonstrated by the Barrow agegraphic dark energy (BADE) model and its modified form, the new Barrow agegraphic dark energy (NBADE) model. However, constraints on the parameters of these models remain uncertain, necessitating the use of robust observational data to gain further insight. Thus, inspired by previous work, this research aims to improve the understanding of these models by using parameter estimation techniques to constrain their key parameters.

We extend the standard analysis by considering both the interacting and non-interacting cases between the two sectors-dark energy and dark matter-within the framework of Barrow entropy. Interacting dark energy (IDE) theories are further supported by the following arguments:

- They could help solve the coincidence problem by explaining why the development of structures on a large scale roughly corresponds to the dominance of dark energy.
- IDE affects structure formation, offering an innovative way to alter the predictions of the conventional non-interacting model [43].

Despite the general consensus that early Universe curvature inhomogeneities were eliminated by inflation, observable data indicate that a slight but non-negligible spatial curvature may still exist [44,45]. For this reason, the background of our analysis is a nonflat FRW Universe. The inclination toward a closed universe emerged from a series of CMB experiments [46–49]. This idea has been supported by WMAP's increased precision, which suggests a modest preference for a closed universe with positive spatial curvature [50–52]. Beyond CMB, recent supernova observations investigating the cubic correction to the luminosity distance [53,54] also show a slight inclination towards a closed universe. Through this comprehensive approach, we aim to provide important perspectives on the characteristics of dark energy, its interaction dynamics, and its impact on the thermal history and future evolution of the universe.

The structure of the paper is as outlined below: in Sect. 2, the field equations and the basic background equations are discussed. In Sect. 3, the condition of thermal stability is described. Next, in Sect. 4, the Swampland conjecture is considered. In Sect. 5, we present our approach to restricting parameters through observational datasets. Section 6 is focused on the investigation of the Barrow agegraphic dark energy (BADE) model, both for non-interacting and interacting cases. The new Barrow agegraphic dark energy (NBADE) model is investigated for interacting and non-interacting cases in Sect. 7. The results of the study are presented in Sect. 8, and linear perturbation analysis is presented in Sect. 9. Finally, all the results are discussed and interpreted in the concluding part, Sect. 10.

2 Field equations

The metric for spherically symmetric, isotropic, homogeneous, spatially non-flat Robertson–Walker geometry takes form [55]

$$ds^2 = -dt^2 + a(t)^2\left[\frac{dr^2}{1-kr^2} + r^2(sin^2\theta d\phi^2 + d\theta^2)\right] \quad (6)$$

where the curvature constant k can be 0, 1, or -1, corresponding to flat, closed, and open geometries, respectively, with $a(t)$ serving as the scale factor.

In the general theory of relativity, the Einstein field equations for FRW metric is

$$R_{\mu\nu} - \frac{1}{2}Rg_{\mu\nu} = T_{\mu\nu} \quad (7)$$

where the energy moment tensors $T_{\mu\nu}$ of the different universal components, including dark energy, dark matter, baryons, and radiation, are represented by the RHS of the above equation, while the LHS of the equation indicates the universe's geometry.

The independent field equations will be

$$3M_p^2\left[H^2 + ka^{-2}\right] = \rho_r + \rho_b + \rho_m + \rho_d = \rho_T \quad (8)$$

$$-M_p^2\left[H^2 + ka^{-2} + 2\frac{\ddot{a}}{a}\right] = p_r + p_b + p_m + p_d = p_T \quad (9)$$

where $\rho_r,\rho_b,\rho_m,\rho_d$ and p_r,p_b,p_m,p_d are energy densities and pressure corresponding to radiation, baryons, matter, dark energy component respectively. The Hubble parameter H,is given by $H = \frac{\dot{a}}{a}$

According to the Bianchi identity $G_{ij}^{;j} = 0$ (where $G_{ij}^{;j}$ is Einstein tensor) leads to $T_{ij}^{;j} = 0$ provides the continuity equation as follows

$$\dot{\rho}_{total} + 3H(\rho_{total} + p_{total}) = 0 \tag{10}$$

In this work, we investigate the gravitational interactions between dark energy and dark matter, the two main components that dominate the universe, and find that the continuity equation for each component reduces to

$$\dot{\rho}_r + 3H(\rho_r + p_r) = 0 \tag{11}$$
$$\dot{\rho}_b + 3H(\rho_b + p_b) = 0 \tag{12}$$
$$\dot{\rho}_m + 3H(\rho_m + p_m) = Q(t) \tag{13}$$
$$\dot{\rho}_d + 3H(\rho_d + p_d) = -Q(t) \tag{14}$$

In these equations, $Q(t)$ denotes the rate of energy interchange between the two dark sections; the transmission of energy therefrom the dark energy to the dark matter section is implied if $Q(t) < 0$, and the inverse is implied if $Q(t) > 0$ [56]. Even though the exact nature of $Q(t)$ is still uncertain; we must assume a specific probable form of $Q(t)$ to study the interaction among the dark sections.

Here, we took the following form of the interaction term $Q(t)$

$$Q(t) = 3f^2H(\rho_d + \rho_m) \tag{15}$$

Here, f^2 represents a dimensionless quantity that denotes the interplay between the two dark sections. The choice of Q in this form is motivated by physical considerations: based on the energy conservation equations, the Hubble parameter H, which has units of inverse time, must be multiplied by the energy densities to represent the interplay between dark energy and dark matter. In literature, there are several arbitrary ways to model Q, with one common choice being $Q \propto H\rho$, where ρ can represent ρ_m,ρ_d,$\rho_m + \rho_d$. Other interaction terms can also be found in the literature used for investigating the universe's dynamical properties, and a comprehensive review is available in [57]. The form of Q, as given in Eq. 15, is a linear combination of energy densities, which simplifies calculations and is suitable for our current study. In the context of energy conservation equations, the inclusion of the interaction term Q ensures the cosmos's total energy remains preserved, even when energy is exchanged between components such as dark energy and dark matter. The interaction term proportional to H reflects the natural coupling between the expansion rate and the energy densities. This coupling could play a significant role in explaining the accelerated expansion of the cosmos. Since the Hubble parameter, H has units of inverse time and is related to the rate of cosmic expansion, $Q(t) = 3f^2H(\rho_d + \rho_m)$ naturally scales with the expansion rate. This shows how the interaction term is influenced by the universe's dynamic evolution. The same interaction term as Eq. (15) was taken in reference [58] to study an interacting model of holographic dark energy using observational data.

Solving the Eq. (11) and using the fact that $\omega_r = \frac{1}{3}$, we can get

$$\rho_r = c_1 a^{-4} \tag{16}$$

Similarly from Eq. (12) and using $p_b = 0$, we can obtain

$$\rho_b = c_2 a^{-3} \tag{17}$$

where c_1 and c_2 are integrating constants.

Now from the Eq. (8), we can obtain

$$\Omega_r + \Omega_b + \Omega_m + \Omega_d - \Omega_k = 1 \tag{18}$$

The fractional energy densities take the form

$$\Omega_r = \frac{\rho_r}{3M_p^2H^2}, \Omega_b = \frac{\rho_b}{3M_p^2H^2}, \Omega_m = \frac{\rho_m}{3M_p^2H^2}, \tag{19}$$

$$\Omega_d = \frac{\rho_d}{3M_p^2H^2}, \Omega_k = \frac{k}{a^2H^2} \tag{20}$$

In view of the Eqs. (16) and (17) we obtain

$$\Omega_r = \Omega_{r_0}\frac{H_0^2}{H^2}(1+z)^4 \; and \; \Omega_b = \Omega_{b_0}\frac{H_0^2}{H^2}(1+z)^3 \tag{21}$$

where Ω_{r_0}, Ω_{b_0} and H_0 are the current value of the respective cosmological parameters.

Now differentiating (8) with respect to t and after some simplification, we can get

$$\frac{\dot{H}}{H^2} = \Omega_k - \frac{3}{2}\left[\frac{4}{3}\Omega_r + \Omega_b + \Omega_m + \Omega_d(1+\omega_d)\right] \tag{22}$$

Also using the fact $q = -1 - \frac{\dot{H}}{H^2}$ we can *express* q the deceleration parameter as follows

$$q = -1 - \Omega_k + \frac{3}{2}\left[\frac{4}{3}\Omega_r + \Omega_b + \Omega_m + \Omega_d(1+\omega_d)\right] \tag{23}$$

3 Thermal stability

Now, let's examine our model through the lens of thermodynamics. Numerous scholarly works have demonstrated that the presence of dark energy in the contemporary accelerating cosmos necessitates the fulfillment of thermal stability conditions. Research suggests that the models of dark energy with two free parameters exhibit greater flexibility with respect to the thermal stability requirement as compared to models with just one free parameter [59–61]. Also, the thermodynamic study of dark energy (DE) offers key insights into its enigmatic nature, as thermodynamic laws universally constrain physical processes. Analyzing the behavior of cosmic fluids may reveal clues about DE. Barboza et al. [61] examined DE fluids, emphasizing the need for positive heat capacities and

Table 1 Stability requirements for the system [62]

Restriction on ω_T	Condition for stability
$\omega_T > 0$	$V\frac{d\omega_T}{dV} < \omega_T^2$ or $V\frac{d\omega_T}{dV} > \omega_T(1+\omega_T)$
$-1 < \omega_T < 0$	$\omega_T(1+\omega_T) < V\frac{d\omega_T}{dV} < \omega_T^2$
$\omega_T < -1$	Unstable

compressibility for stability. They concluded that a stable DE fluid requires the equation of state parameter to be a negative constant, which conflicts with constraints derived from observational data, including Type Ia supernovae, H(z), and BA measurements.

Inspired by all of the findings, we will look into whether our model satisfies the thermal stability requirements. Specifically, we utilize the analysis of [62–64], to check the thermal stability condition (TSC). The thermal stability of our models was assessed using the final deduced conditions provided in previously mentioned references rather than performing detailed derivations. This approach aligns our analysis with prior work, and leverages established results for efficiency and consistency.

Our model will meet the thermal stability condition (TSC) only when the overall EoS parameter w_T adheres to the following inequality stated below

$$\omega_T - \frac{d\ln|\omega_T|}{3\ln a} \geq 0 \tag{24}$$

where $\omega_T = \frac{p_T}{\rho_T}$ and because of the homogenous and isotropic nature of the cosmos, the same factor a is used for scaling all physical lengths. Now ω_T can be found by using the (8) and (9) as follows

$$\omega_T = \frac{\Omega_r + \Omega_d\omega_d}{(1+\Omega_k)} \tag{25}$$

The condition (24) is valid for any range of ω_T and provides a general criterion for thermal stability. While this inequality gives a broad assessment of stability, we included Table 1 to present a more detailed analytical comparison based on different ranges of ω_T. The table outlines the specific stability criteria depending on whether ω_T is positive, negative but greater than -1, or less than -1.

- V ($V \propto a^3$) represents the volume of the universe, and $\frac{d\omega_T}{dv}$ denotes the derivative of the EoS parameter with respect to volume.
- The condition $\omega_T > 0$ suggests that the system can be stable if the derivative of ω_T relative to volume meets one of the specified inequalities. This range typically corresponds to stiff fluid or radiation-like behavior, which is less relevant for dark energy models.
- For $-1 < \omega_T < 0$, the stability condition suggests that quintessence-like dark energy could potentially maintain stability, provided that the change satisfies the specified bounds. This range is of particular interest as it allows for a dynamical dark energy scenario, which is consistent with the behavior observed in our model for certain parameter values.
- If $\omega_T < -1$, the system is deemed unstable, indicating that a phantom-like behavior leads to a violation of thermal stability. This scenario is associated with negative heat capacities and violations of the second law of thermodynamics, making it theoretically problematic. To provide a more cohesive presentation of the results, we now link the analytical derivation of TSC to the graphical analysis in Sect. 8, presenting a visual representation of how the TSC behaves across different redshift values. This approach allows us to directly observe whether the stability condition is met or violated in various phases of the cosmic evolution.

4 Swampland conjucture

In terms of the phenomenology of quantum gravity theories, the swampland programmer is a fascinating new advancement, as it accurately links to questions concerning effective field theories and their UV completions. The most well-known theory of quantum gravity is string theory, which is thought to have been developed using consistent low-energy effective field theories in order to build consistent quantum gravity theory. However, there is another huge landscape beyond these string landscapes where seemingly consistent effective field theories are actually incompatible with quantum gravity theory. In order to ensure that consistent, effective field theories are not located in the swampland, we eventually need a set of conjectures. The excitement primarily stemmed from the observation that exact de-sitter solutions involving non-negative cosmological parameters are incompatible with the string landscape, posing significant challenges in linking high-energy frameworks to fundamental theories.

We also discover that early-period inflationary theories typically contradict the swampland conjecture, whereas the later-stage quintessence model simultaneously satisfies this conjecture and the existing conservational facts. Using the dark energy quintessence model, recent work [65] has developed the swampland criterion as the string theory bound. The Swampland conjecture concerning the viability of the modified theory of gravity $f(R)$ theory, $f(R,T)$ was recently examined by [66]. Many works, notably [67–69], used the Swampland criterion to link DE quintessence models. In this section, we will explore and clarify the relationship between the refined swampland program conjecture and dark energy.

The conjectures relate to models of dark energy that are associated with a scalar field ϕ, where the field's potential $v(\phi)$ corresponds to the energy density of dark energy, mak-

ing the field ϕ a potential source of dark energy. This section explores the scalar field and its associated potential in the quintessence model and consider the following equations

$$\rho = \frac{1}{2}\dot{\phi}^2 + v(\phi) \tag{26}$$

$$p = \frac{1}{2}\dot{\phi}^2 - v(\phi) \tag{27}$$

Solving these two equations, we can get

$$v(\phi) = \frac{1}{2}(1 - \omega_{DE})\rho_{DE} \quad and$$

$$\dot{\phi}^2 = \frac{1}{2}(1 + \omega_{DE})\rho_{DE} \tag{28}$$

The swampland criteria consist of two main conjectures in the context of string theory and cosmology. These criteria impose a minimum constraint on $\frac{\phi V}{V}$ for $V > 0$ and a maximum limit on the distance traversable by scalar fields. It is observed that specific quintessence models are capable of satisfying these constraints when applied to current dark energy and argue that if both Swampland conditions hold, the universe will transition phases within a few Hubble times. Motivated by this, the author of [70] proposes the refined swampland conjecture in the following form.

- Swampland criterion 1:

$$\frac{|V'|}{V} > C_1 M_p \tag{29}$$

- Swampland criterion 2:

$$\frac{|V''|}{V} < -C_2 M_p^2 \tag{30}$$

where C_1 and C_2 are constants of unit order. To understand the nature of dark energy, we treat the scalar field ϕ as its only energy source, playing the role of the quintessence model. In this framework, we have analyzed our model in the context of the Swampland conjecture.

5 Methodology

This section first presents the dataset that was utilized for the observational study, after which we describe the statistical techniques that were employed. In both interacting and non-interacting scenarios, we have applied Markov Chain Monte Carlo (MCMC) [71] analysis to restrict the parameters of the NBADE and BADE models. The dataset includes 31 data points from the observational Hubble data (OHD) and 26 data points from Baryon Acoustic Oscillation (BAO) measurements, making a total of 57 data points covering a broad range of redshifts from $0.106 < z < 2.36$. These data points have been thoroughly discussed by Sharov and Vasiliev in the referenced work [72]. The complete dataset of CC+BAO is provided in the Table 2.

We may effectively explore the parameter space and get samples of the probability distributions for each parameter by utilizing the Markov Chain Monte Carlo (MCMC) approach within the Bayesian framework [73,74]. To assess how well the model predictions match the observational data, this statistical method makes use of likelihood functions. The Bayesian approach provides numerous benefits, such as incorporating prior knowledge or constraints from earlier studies and effectively managing uncertainties in both the model and observational data. The best-fit values and corresponding uncertainties of the model parameters are listed in Tables 3 and 4. As a concluding step, we employ the Akaike information criterion (AIC) [75], the Bayesian information criterion (BIC) [76] to analyze the quality of the fittings and determine the observational consistency of the scenarios. The AIC is derived from information theory and functions as an estimator for the Kullback–Leibler information, characterized by its asymptotic unbiasedness. Under the assumption of Gaussian errors, the corresponding estimator can be written as:

$$AIC = -2ln(\mathcal{L}_{max}) + 2k + \frac{2k(k+1)}{N_{tot} - k - 1} \tag{31}$$

where $\mathcal{L}_{max}$ and N_{tot} denotes the maximum likelihood and the number of total points in the datasets. Conversely, the BIC criterion acts as an estimator of the Bayesian evidence, which can be represented as:

$$BIC = -2ln(\mathcal{L}_{max}) + klog(N_{tot}) \tag{32}$$

To compare a set of n models, we employ the criteria mentioned above by calculating the relative difference of the involved information criteria, defined as $IC_{model} = IC_{model} - IC_{min}$, where IC_{min} represents the minimum information criterion value within the set of models being compared [19]. Employing the Jeffreys scale [77], the ΔIC values are interpreted as follows: a $\Delta IC \leq 2$ suggests that the model being analyzed is statistically compatible with the reference model. A $2 \leq \Delta IC \leq 6$ value between 2 and 6 indicates moderate tension between the two models, while a $\Delta IC \geq 10$ reflects strong tension between them. In Table 5, we provide the relevant values for our models.Relative support for various models is measured by the ΔAIC and ΔBIC; lower values of these metrics suggest higher likelihood and better model fit. In order to help researchers choose the best cosmological models, these criteria provide a means of balancing model complexity and goodness of fit.

When fitting models to data, determining which parameters provide the best fit is not enough; we also need to determine whether the best fit is a good fit. To obtain approximate goodness of fit metric, we calculate reduced chi-squared,

which can be described as

$$\chi^2_{red} = \frac{\chi^2}{N_{tot} - k} \tag{33}$$

A reduced chi-squared significantly less than 1 suggests that the error bars are most likely overestimated (too big) or that our model has too many parameters, for a good fit we must have $\chi^2_{red} \approx 1$ conversely, a reduced chi-squared that is significantly more than 1 suggests that our model is not well suited to the data.

5.1 Data description

5.1.1 Cosmic chronometers

Cosmic chronometers (CC) data provide measurements of the Hubble rate based on the estimation of differential age between galaxies that are evolving passively and that no longer undergo active star formation and are predominantly made up of older star populations [78,79]. By assessing the age and metallicity of these nearby galaxies, we can estimate the rate of expansion of $H_{CC}(z)$ at a particular redshift z_{CC}. This estimate comes from the concept that the rate of the expansion can be estimated as the ratio of the change in redshift to the change in time, adjusted for the redshift:

$$H_{CC} \equiv -\frac{1}{1 + z_{CC}} \frac{dz_{CC}}{dt} \tag{34}$$

We compile cosmic chronometer observations from several sources that span the redshift range $0.07 \leq z \leq 1.97$, *as outlined in* [80,81]. From a cosmological perspective, it is noteworthy that the cosmic chronometer (CC) data are model-independent as long as we operate within FRW (Friedmann–Robertson–Walker) spacetime without any additional extrinsic curvature.

5.1.2 Baryon acoustic oscillations

In our current study, we choose a subset of data points from the BAO measurements, which are obtained from 111 various galaxy survey experiments. The Sloan Digital Sky Survey (SDSS) [82,83] is the primary source of most of these data points. We also include measurements from the 6dFGS BAO survey [84,85], the Dark Energy Camera Legacy Survey (DECaLS) [86,87], and the Dark Energy Survey (DES) [88]. The BAO data can be represented as

$$D_A = \frac{D_M}{1 + z} \tag{35}$$

where the cosmological observables D_A is the angular diameter distance and D_M is the comoving angular diameter dis-

Table 2 Cosmic chronometers and baryon acoustic oscillation dataset

z	$H(z)$ [km/s/Mpc]	Error [km/s/Mpc]
0.07	69.0	19.6
0.09	69.0	12.0
0.12	68.6	26.2
0.17	83.0	8.0
0.1791	75.0	4.0
0.1993	75.0	5.0
0.2	72.9	29.6
0.24	79.69	2.99
0.27	77.0	14.0
0.28	88.8	36.6
0.3	81.7	6.22
0.31	78.18	4.74
0.34	83.8	3.66
0.35	84.7	9.1
0.3519	83.0	14.0
0.36	79.94	3.37
0.38	81.5	1.9
0.3802	83.0	13.5
0.4	95.0	17.0
0.4	82.04	2.03
0.4004	77.0	10.2
0.4247	87.1	11.2
0.43	86.45	3.97
0.44	82.6	7.8
0.44	84.81	1.83
0.4497	92.8	12.9
0.47	89.0	34.0
0.4783	80.9	9.0
0.48	97.0	62.0
0.48	87.79	2.03
0.51	90.4	1.9
0.52	94.35	2.64
0.56	93.34	2.3
0.57	87.6	7.8
0.57	96.8	3.4
0.59	98.48	3.18
0.593	104.0	13.0
0.6	87.9	6.1
0.61	97.3	2.1
0.64	98.82	2.98
0.6797	92.0	8.0
0.73	97.3	7.0
0.7812	105.0	12.0
0.8754	125.0	17.0
0.88	90.0	40.0

Table 2 continued

z	$H(z)$ [km/s/Mpc]	Error [km/s/Mpc]
0.9	117.0	23.0
1.037	154.0	20.0
1.3	168.0	17.0
1.363	160.0	33.6
1.43	177.0	18.0
1.53	140.0	14.0
1.75	202.0	40.0
1.965	186.5	50.4
2.3	224.0	8.6
2.33	224.0	8.0
2.34	222.0	8.5
2.36	226.0	9.3

tance given by

$$D_M = \frac{c}{H_0}\int_0^z \frac{dz'}{E(z')} \tag{36}$$

H_0 is the present value and $E(z)$ is the dimensionless value of the Hubble parameter.

Using Python and the emcee library, we created our MCMC algorithm. The likelihood function was developed, assuming that the observational data contained Gaussian errors. For the model parameters, we chose uniform prior distributions that were limited by physically motivated constraints. After a 200-step burn-in phase, the MCMC chains were run for 2500 steps to guarantee convergence. We used around 35 walkers to effectively investigate the parameter space.

We calculate the chi-squared distance χ^2 to evaluate the agreement between theoretical predictions and data at various redshifts:

$$\chi^2 = \sum_{i=1}^{57} \frac{(H_{th}(z_i) - H_{obs}(z_i))^2}{\sigma^2_{H(z_i)}} \tag{37}$$

for each data point at redshift z_i, where $\sigma_{H(z)i)}$ is the standard deviation, H_{obs} is the observed values, and H_{th} is the model predictions.

6 BADE

The energy density for the Barrow holographic dark energy model is

$$\rho_d = BL^{\Delta-2} \tag{38}$$

where B is a parameter of dimension $L^{-\Delta-2}$ and L is the infrared (IR) cut-off.

Taking the Universe's age T as the IR cut-off, we get the energy density for Barrow agegraphic dark energy (BADE) [5], as

$$\rho_d = cT^{\Delta-2} \tag{39}$$

where T can be defined as

$$T = \int_0^a dt = \int_0^a \frac{da}{Ha} \tag{40}$$

Clearly,$\dot{T} = 1$. Therefore we get

$$\dot{\rho}_d = (\Delta - 2)\frac{\rho_d}{T} \tag{41}$$

Hence, using equation (19) we get

$$T = \left(\frac{3M_p^2H^2}{c}\Omega_d\right)^{\frac{1}{\Delta-2}} \tag{42}$$

Now, differentiating the above equation with respect to cosmic time t, we obtain

$$\dot{T} = \frac{T}{\Delta-2}\left[\frac{2H\dot{H}\Omega_d + H^2\dot{\Omega}_d}{H^2\Omega_d}\right] \tag{43}$$

Finally, on using the Eqs. (41) and (43), we can obtain

$$\dot{\rho}_d = \rho_d\left[2\frac{\dot{H}}{H} + \frac{\dot{\Omega}_d}{\Omega_d}\right]. \tag{44}$$

6.1 Non-interacting case

In this scenario, the dark sectors of the universe do not interact with each other; hence, Q=0. Now, using Eqs. (14) and (41), we can find ω_d as

$$\omega_d = -1 - \frac{\Delta-2}{3HT} \tag{45}$$

Equations (22) and (23) in this case are obtained by using as

$$\frac{\dot{H}}{H^2} = -\frac{k(1+z)^2}{2H^2} - \frac{\Omega_{r_0}H_0^2(1+z)^4}{2H^2} - \frac{3(1-\Omega_d)}{2} + \frac{\Omega_d(\Delta-2)}{2HT} \tag{46}$$

$$q = -\frac{1}{2} - \frac{3\Omega_d}{2} - \frac{\Omega_d(\Delta-2)}{2HT} + \frac{\Omega_k}{2} + \frac{\Omega_{r_0}H_0^2(1+z)^4}{2H^2} \tag{47}$$

Additionally,it requires investigation to ascertain $\dot{\Omega}_d$

$$\dot{\Omega}_d = 2H\Omega_d(1+q) + \frac{\Omega_d(\Delta-2)}{T} \tag{48}$$

The continuity Eq. (14) and the relation (41) have been used to derive it. We numerically solve this equation to ascertain the behavior of BADE for non-interacting cases with the two initial conditions H=67 and $\Omega_d = 0.7$ at $z = 0$.

Table 3 MCMC results and priors for BADE model for interacting and non-interacting cases

Model	Parameter	MCMC result	Priors
BADE	H_0	$67.3618285 \pm 1.95471596$	[50, 80]
	Ω_{m0}	$0.26364926 \pm 0.01277081$	[0.25, 0.35]
	Ω_{r0}	$0.00044657 \pm 0.00034756$	[0.00001, 0.001]
	Ω_{b0}	$0.00369755 \pm 0.00336605$	[0.00001, 0.01]
	Ω_{d0}	$0.63898232 \pm 0.08042561$	[0.5,0.8]
	Δ	$0.38920949 \pm 0.34208382$	[0, 1.0]
BADEI	H_0	$69.9216662 \pm 0.80655578$	[67,150]
	Ω_{d0}	$0.62890544 \pm 0.02582694$	[0.6, 2]
	Ω_{r0}	$0.00028104 \pm 0.00021140$	[0.0000001, 0.0006]
	Ω_{b0}	$0.00044021 \pm 0.00029137$	[0.00001, 0.0009]
	Δ	$0.05226922 \pm 0.03363074$	[0, 0.1]
	f	$0.04865782 \pm 0.03278573$	[0.00001,2]
ΛCDM	H_0	$69.7928466 \pm 1.10248203$	[40, 80]
	Ω_{m0}	$0.26913846 \pm 0.01787429$	[0.01, 0.4]

Table 4 MCMC results and priors for NBADE model for interacting and non-interacting cases

Model	Parameter	MCMC result	Priors
NBADE	H_0	$67.7503213 \pm 1.99877426$	[50, 80]
	Ω_{m0}	$0.26247749 \pm 0.01220351$	[0.25, 0.35]
	Ω_{r0}	0.0004777 ± 0.00031211	[0.00001, 0.001]
	Ω_{b0}	$0.00322936 \pm 0.00320434$	[0.00001, 0.01]
	Ω_{d0}	$0.65938299 \pm 0.08711292$	[0.5,0.8]
	Δ	$0.46843207 \pm 0.34722287$	[0, 1.0]
NBADEI	H_0	$68.0013342 \pm 0.92303832$	[67,150]
	Ω_{d0}	$0.66199817 \pm 0.04389439$	[0.3, 0.81]
	Ω_{r0}	$0.00029138 \pm 0.00019873.$	[0.0000001, 0.0006]
	Ω_{b0}	$0.00039903 \pm 0.00029321$	[0.00001,0.0009]
	Δ	$0.05353258 \pm 0.03310451$	[0, 0.1]
	f	$0.02656464 \pm 0.02719395$	[0.00001,2]
ΛCDM	H_0	$69.7928466 \pm 1.10248203$	[40, 80]
	Ω_{m0}	$0.26913846 \pm 0.01787429$	[0.01, 0.4]

Table 5 AIC, BIC and χ^2 values for the different models and their differences with respect to the ΛCDM model

Model	AIC	ΔAIC	BIC	ΔBIC	χ^2_{min}	χ^2_{red}
ΛCDM	−28.625	0	−24.539	0	32.159	0.584
$BADE$	−22.553	6.071	−10.295	14.243	18.843	0.523
$NBADE$	−22.359	6.266	−10.100	14.438	22.302	0.543
$BADEI$	−18.485	10.140	−6.226	18.312	33.388	0.654
$NBADEI$	−18.117	10.507	−5.859	18.680	33.604	0.658

6.2 Interacting case

We now extend the earlier analysis to take into account the scenario in which the interaction (15) between the dark sectors of the universe is taken into account. We get the following generalized formula for the EoS parameter using the same computations as previously.

$$\omega_d = -1 - f^2(1+\frac{\Omega_m}{\Omega_d}) - \frac{\Delta-2}{3HT} \tag{49}$$

Now similarly using Eqs. (22) and (23) , we get

$$\frac{\dot{H}}{H^2} = -\frac{k(1+z)^2}{2H^2} - \frac{\Omega_{r_0}H_0^2(1+z)^4}{2H^2} - \frac{3(1-\Omega_d)}{2} + \frac{3\Omega_d}{2}\left(f^2\left(1+\frac{\Omega_m}{\Omega_d}\right)+\frac{\Delta-2}{3HT}\right) \tag{50}$$

Furthermore,

$$\dot{\Omega}_d = 2H\Omega_d(1+q) + \frac{\Omega_d(\Delta-2)}{T} \tag{51}$$

We solve this equation numerically with the two initial conditions H=67 and $\Omega_d = 0.7$ at $z = 0$ to determine the behavior of BADE in interacting scenarios.

7 NBADE (new Barrow agegraphic dark energy)

To address certain issues in the original agegraphic dark energy (ADE) model, Wei and Cai proposed a new agegraphic dark energy model by using η (the conformal time) as the infrared cut-off instead of the age of the universe. Here, η is interpreted as $ad\eta = dt$ i.e. $\dot{\eta} = \frac{1}{a}$

$$\eta = \int_0^a \frac{da}{a^2 H} \tag{52}$$

The energy density of NBADE can be expressed in this manner

$$\rho_d = c\eta^{\Delta-2} \tag{53}$$

7.1 Non-interacting case

Here, Q = 0.

Now using the Eq. (14) we can find ω_d as

$$\omega_d = -1 - \frac{\Delta-2}{3Ha\eta} \tag{54}$$

Also, by using this equation, Eqs. (22) and (23) become

$$\frac{\dot{H}}{H^2} = -\frac{\Omega_k}{2} - \frac{\Omega_{r_0}H_0^2(1+z)^4}{2H^2} - \frac{3}{2}(1-\Omega_d) + \frac{\Omega_d(\Delta-2)}{2Ha\eta} \tag{55}$$

$$q = -\frac{1}{2} - \frac{3\Omega_d}{2} - \frac{\Omega_d(\Delta-2)}{2Ha\eta} + \frac{\Omega_k}{2} + \frac{\Omega_{r_0}H_0^2(1+z)^4}{2H^2} \tag{56}$$

Additionally,it requires investigation to ascertain $\dot{\Omega}_d$

$$\dot{\Omega}_d = 2H\Omega_d(1+q) + \frac{\Omega_d(\Delta-2)}{a\eta} \tag{57}$$

7.2 Interacting case

We further expand the preceding analysis to the scenario of accounting for the interaction (15) between the universe's dark regions. Following the same approach as above, we can derive the required equations for this case as follows.

$$\omega_d = -1 - f^2(1+\frac{\Omega_m}{\Omega_d}) - \frac{\Delta-2}{3Ha\eta} \tag{58}$$

Now similarly using Eqs. (22) and (23) we get

$$\frac{\dot{H}}{H^2} = -\frac{k(1+z)^2}{2H^2} - \frac{\Omega_{r_0}H_0^2(1+z)^4}{2H^2} - \frac{3(1-\Omega_d)}{2} + \frac{3\Omega_d}{2}\left(f^2\left(1+\frac{\Omega_m}{\Omega_d}\right)+\frac{\Delta-2}{3Ha\eta}\right) \tag{59}$$

Furthermore,

$$\dot{\Omega}_d = 2H\Omega_d(1+q) + \frac{\Omega_d(\Delta-2)}{a\eta} \tag{60}$$

Now, we need to solve these equations numerically to determine the other cosmological parameters.

8 MCMC results and cosmographic parameter analysis

It is crucial to compare our new parametrizations in BADE, BADEI, NBADE, NBADEI with the widely employed ΛCDM model in order to comprehend deviations and learn more about the dynamics of the Universe.According to our research, in the non-interacting condition, the ΛCDM model yields higher values for the Hubble constant (H_0) than do the BADE and NBADE models. For the model of BADE and NBADE, the Hubble parameter values are $67.3618285 \pm 1.95471596\, kms^{-1}\, Mpc^{-1}$ and $67.7503213 \pm 1.99877426\, kms^{-1}\, Mpc^{-1}$, respectively. However, the H_0 values in the BADEI and NBADEI cases are closer to the ΛCDM model's H_0value.For BADEI H_0 is $69.9216662 \pm 0.80655578\, kms^{-1}\, Mpc^{-1}$ and for NBADEI the value is $68.0013342 \pm 0.92303832\, kms^{-1}\, Mpc^{-1}$ .These values are consistent with the Planck Collaboration value [89], but they differ from the SH0ES Collaboration 2019 value [90]. To investigate the parameter degeneracies and confidence intervals, we generated 2D marginalized contour plots for all our models using GetDist in Figs. 1 and 2. These plots illustrate the interplay between two cosmological parameters at a

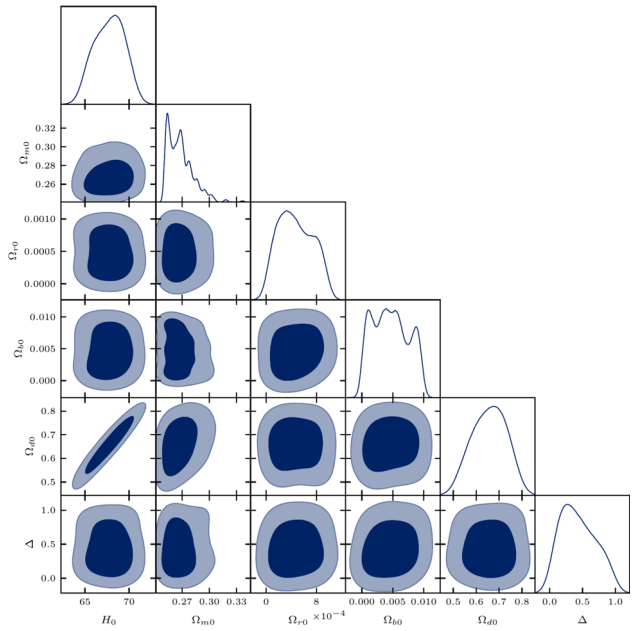

(a)

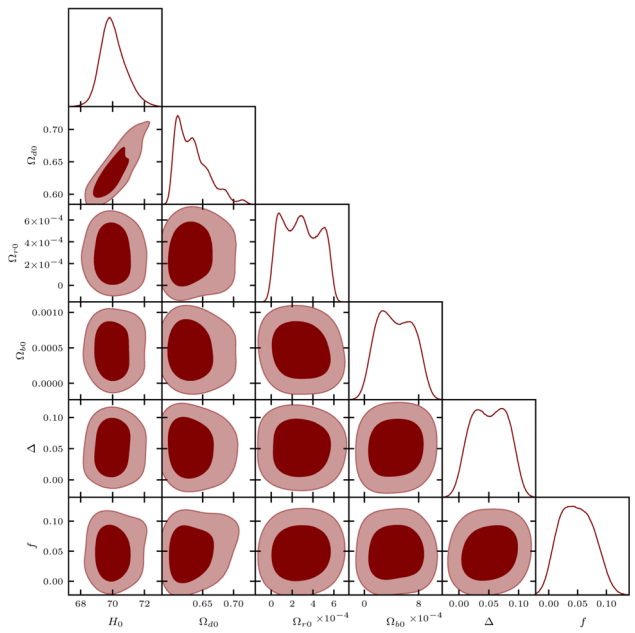

(b)

Fig. 1 Posterior distribution of BADE model parameters fig: (**a**) for non-interacting and fig: (**b**) interacting case at 1σ and 2σ confidence level

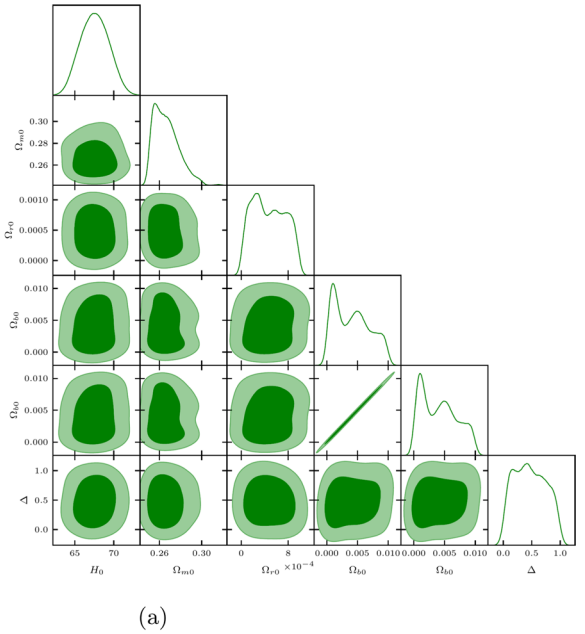

(a)

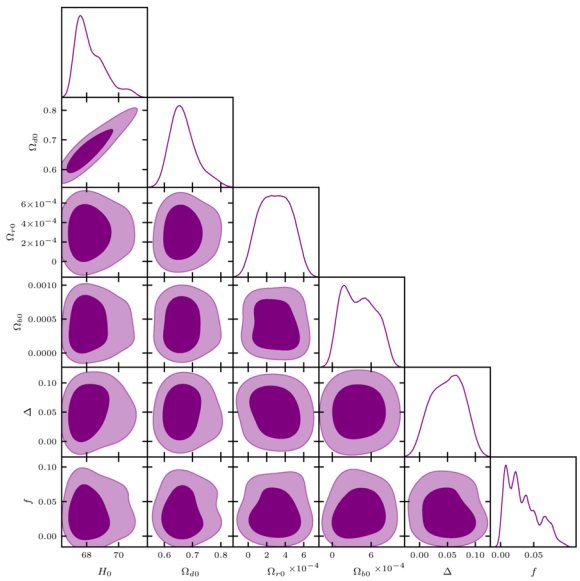

(b)

Fig. 2 Posterior distribution of NBADE model parameters for fig: (**a**) non-interacting and fig: (**b**) interacting case at 1σ and 2σ confidence level

time, highlighting the 68% and 95% confidence regions. The Hubble rate $H(z)$ evolution as a function of redshift z for two different models-the ΛCDM model and the new model-in the context of BADE and NBADE in both interacting and non-interacting scenarios is depicted in Figs. 3 and 4. In the CC+BAO dataset, the data points are shown in blue, and their error bars are shown in green. As the image illustrates, both models exhibit excellent alignment with the ΛCDM model when there is no interaction, but in the case of interaction, both models agree with the reference model at lower redshifts while exhibiting minimal deviation at higher redshifts. These results confirm our parametrizations' efficacy in explaining cosmic expansion by highlighting their satisfactory match with the empirical evidence.

In this work, we parameterized the Barrow exponent Δ in the Barrow agegraphic dark energy (BADE) and new

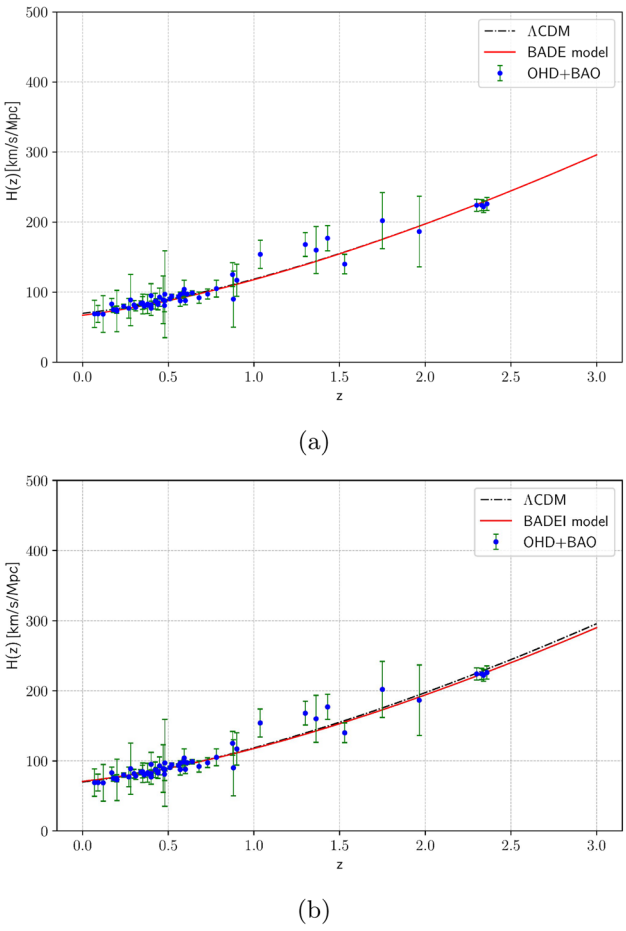

Fig. 3 Comparison of Hubble parameter $H(z)$ between ΛCDM and the BADE model for fig: (**a**) non-interacting and fig: (**b**) interacting case using 57 CC + BAO data points

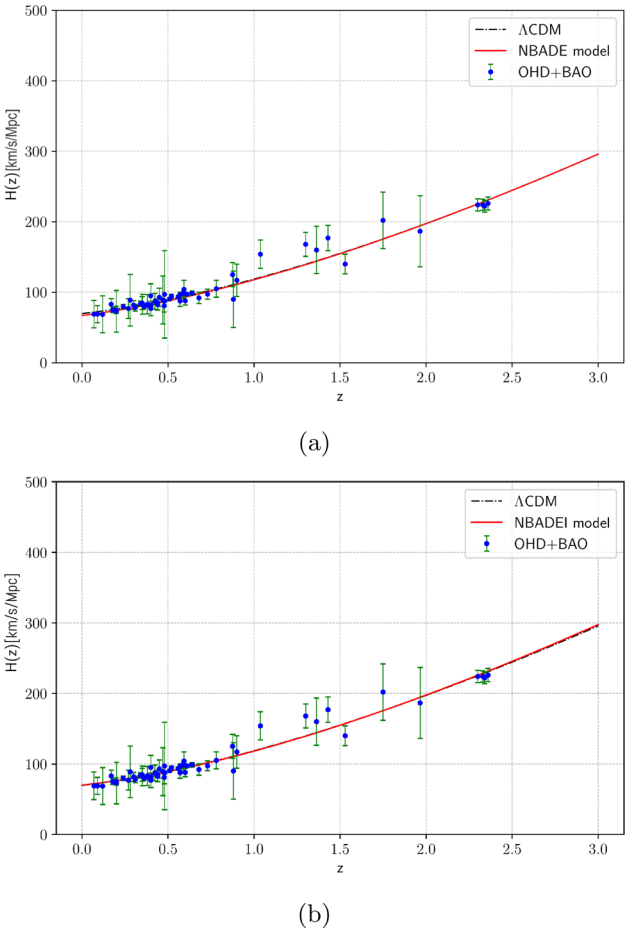

Fig. 4 Comparison of Hubble parameter $H(z)$ between ΛCDM and the NBADE model for fig: (**a**) non-interacting and fig: (**b**) interacting case using 57 CC + BAO data points

Barrow agegraphic dark energy (NBADE) models to better understand dark energy evolution. As suggested by Professor Barrow, we restricted Δ to the range between 0 and 1. We treated Δ as a free parameter with a prior distribution and estimated it using Markov Chain Monte Carlo (MCMC) sampling from observational data. We found that the obtained value of $\Delta = 0.389 \pm 0.342, 0.0522 \pm 0.0336, 0.468 \pm 0.347, 0.0535 \pm 0.0331$ for BADE, BADEI, NBADE, NBADEI models respectively. The values of Δ in the interacting case of both models are very close to the estimate in Reference [91], but it does not, however, fall within the limits $0.005 \leq \Delta \leq 0.008$ [92] and $\Delta \leq 1.4 \times 10^{-4}$ [93], which were obtained from measurements of baryogenesis and Big Bang nucleosynthesis, respectively. As mentioned in [94], this disparity might be reconciled by taking into account an HDE description of the Universe with a running Barrow entropy. The Δ values in the non-interacting case align closely with the results reported in [36,37]. To demonstrate the impact of the Barrow exponent on our model, we considered three distinct values of the model parameter Δ for plotting all the graphs, selecting these values from within the range obtained through parameter estimation. For simplicity in calculations, we assumed $k = 1$, $c = 15$ throughout the entire paper.

Furthermore, the inclusion of the factor f in the interaction term plays a crucial role in refining the model's predictive capability. By allowing for a controlled and systematic interaction, f provides additional flexibility in fitting the observational data and helps capture the complex interplay between dark energy and dark matter. From our parameter estimation, we obtained the value of f as $0.04865782 \pm 0.03278573, 0.02656464 \pm 0.02719395$ for BADEI and NBADEI respectively, demonstrating the subtle yet significant influence of the interaction term on the model's dynamics. The importance of including the interaction term, along with its observational implications, is further elaborated in the conclusion section, where the performance of the models is discussed in the context of key cosmological parameters and statistical criteria.

We present a thorough comparison between the New Models and the ΛCDM Model using the data from Table 5, taking into account a number of statistical measures such as AIC, BIC, ΔAIC,ΔBIC, χ^2_{min} and χ^2_{red}. The χ^2_{min}analysis reveals that the BADE and NBADE models outperform the ΛCDM Model, indicating a superior fit to the data by minimizing the total χ^2. Conversely, the NBADEI and BADEI models show higher χ^2_{min} values compared to the ΛCDM Model, suggesting that ΛCDM offers a better fit in these instances. Overall, the BADE and NBADE models emerge as the most compatible with the observational data, while the NBADEI and BADEI models lag behind in terms of fit quality. A more precise fit to the data is indicated by the BADE and NBADE models χ^2_{red} values, which are lower than those of the ΛCDM, BADEI, and NBADEI models and are around 1. According to AIC, the ΛCDM Model offers a better balance between goodness of fit and model complexity, as evidenced by the New Model's higher AIC value than the ΛCDM model.In comparison to the ΛCDM Model, the New Model appears to have modest support, as indicated by the ΔAIC values for the BADE and NBADE models, which are 6.071 and 6.266, respectively. According to ΔAIC, these values fall between 4 and 7, suggesting a respectable degree of support for the New Models.

The ΔAIC values for the BADEI and NBADEI models are 10.140 and 10.507, respectively, suggesting that the New Model has less support than the ΛCDM Model. The BIC and ΔBIC values for all the models, including BADE, NBADE, BADEI, and NBADEI, are significantly larger compared to the ΛCDM model. This indicates a weaker level of support for these models under the Bayesian framework.

8.1 Cosmographic parameter analysis

From Fig. 5, it is evident that the evolution of ω_d suggests a quintessence ($-1 < \omega_d < -\frac{1}{3}$) dark energy model for each case. It is worth noting that, in the later stages, as ω_d approaches -1, the universe may transition into the era described by the standard ΛCDM model, both in the interacting and non-interacting cases of NBADE. The values of ω_d at the current epoch ($z = 0$), for the BADE, NBADE, BADEI, and NBADEI models are, respectively:$[-0.65345, -0.525938]$, $[-0.64021, -0.53054]$, $[-0.752196, -0.72893]$, $[-0.75046, -0.724042]$ for the specified values of Δ.These theoretical predictions show slight differences from current observational constraints [64]. For the sake of completeness, let's investigate the evolution of the deceleration parameter. The profile of the deceleration parameter in Fig. 6 shows a phase transition from the positive region, indicating deceleration in the early universe, to the negative region, signifying acceleration in the later universe.However, mathematically speaking, the redshift z_t, at which the Universe accelerates from a decelerated state, falls inside the interval $z_t \in [0.26854, 0.72234]$, $z_t \in [0.07123, 0.32941]$, $z_t \in [0.66550, 0.70044]$, $z_t \in [0.45851, 0.544578]$ for the model parameter values taken into consideration for BADE, NBADE, BADEI, NBADEI respectively. These redshift range coincides with the observing limitations from SNIa+BAO/CMB ($z_t = 0.72 \pm 0.05$), SNIa+CMB ($z_t = 0.57 \pm 0.07$), and the combined evaluation of SNIa+CMB+LSS ($z_t = 0.61$) [95] except for the NBADE model where the range is relatively lower compared to other models. Additionally, the deceleration parameter's current value for each model is estimated as $[-0.20847, -0.06179]$ for BADE, $[-0.20647, -0.057282]$ for NBADE, $[-0.29489, -0.26555]$ for BADEI, $[-0.30453, -0.25822]$ for NBADEI, the lower bound is nearer to the experimental value cited in the reference [96]. These findings offer more proof that the models under consideration are consistent with observations. Subsequently, Figs. 7 and 8 discuss the evolution of two more significant cosmological parameters-jerk and snap parameters. Throughout the entire existence of the universe, the evolution of the jerk parameter has remained in the positive region. It is also important to note that the jerk parameter tends toward -1 in the distant future, which aligns with the ΛCDM model for the NBADE and NBADEI models, but shows a discrepancy with the ΛCDM model for the BADE and BADEI models. In the case of the snap parameter, the graphs show a transition from the negative region to the positive region for each case, however it tends toward 1 for the NBADE and NBADEI models, resembling the ΛCDM model.

The statefinder diagnostic pair (r, S) is a common tool in cosmology to study dark energy models. As proposed by Alam et al. [97], and Sahni et al. [98], r is similar to the jerk parameter j, and S is a linear combination of the deceleration parameter q and j. These diagnostic pairs are geometric quantities dependent on the scale factor and its time derivative [99,100]. The statefinder parameters can also be understood as

$$r = q + 2q^2 - \frac{\dot{q}}{H}, \mathbf{S} = \frac{2}{3}(q+1) - \frac{1}{3H}\left(\frac{\dot{q}}{q-0.5}\right) \quad (61)$$

Figure 9 depicts the behavior of the $q-r$ profile in the considered models. In each case, the evolution trajectories begin in the early universe's matter-dominated phase ($q > 0, r > 1$) and eventually transition into the dark energy-dominated quintessence zone ($q < 0, r < 1$). Interestingly, for BADE and BADEI, the trajectories stay in the quintessence zone in the latter phase of the universe's formation. But in the latter stages of NBADE and NBADEI, the trajectories finally arrive at the SS (de Sitter) fixed point ($q = -1, r = 1$). The universe with the de Sitter line has accelerated expansion, and it is dominated by dark energy. The fact that the trajectories never pass through the chaplygin gas area indicates that the model's dominant dark energy component is quintessence.

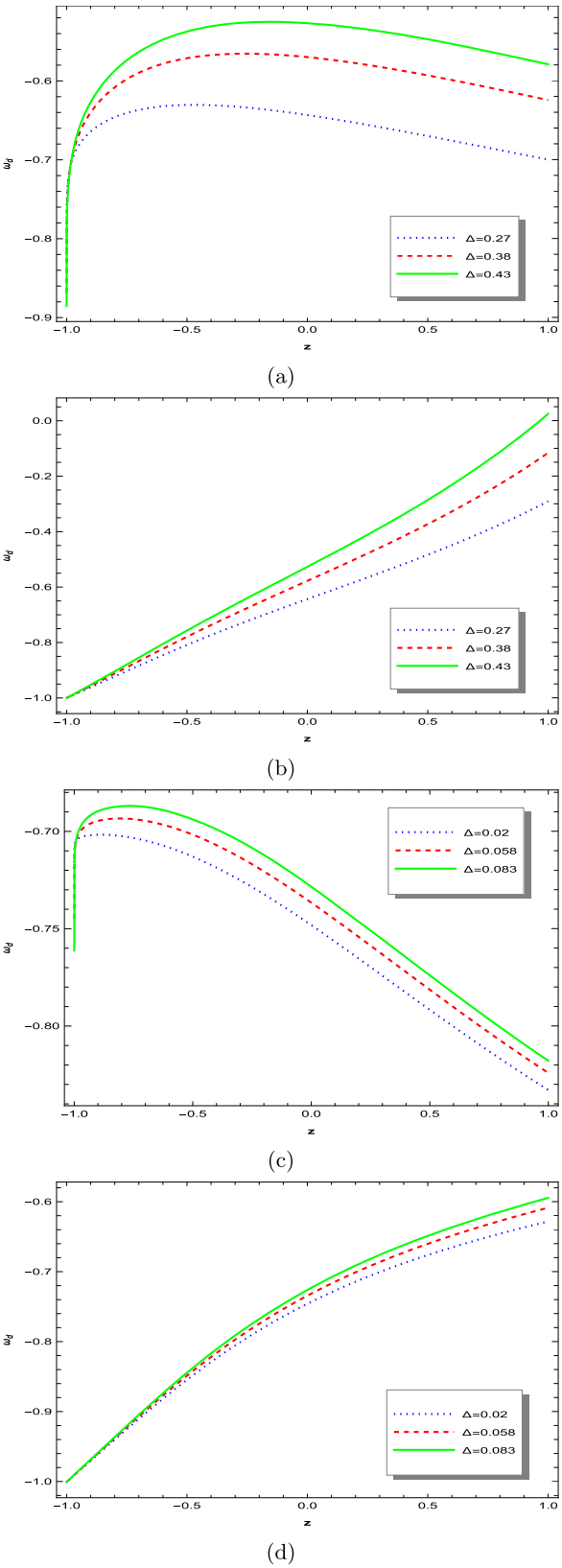

Fig. 5 Variation of the EoS parameter ω_d with redshift z: subfigures display the behavior of $\omega(z)$ for three values of Δ under four distinct scenarios: (**a**) BADE, (**b**) NBADE, (**c**) BADEI, (**d**) NBADEI

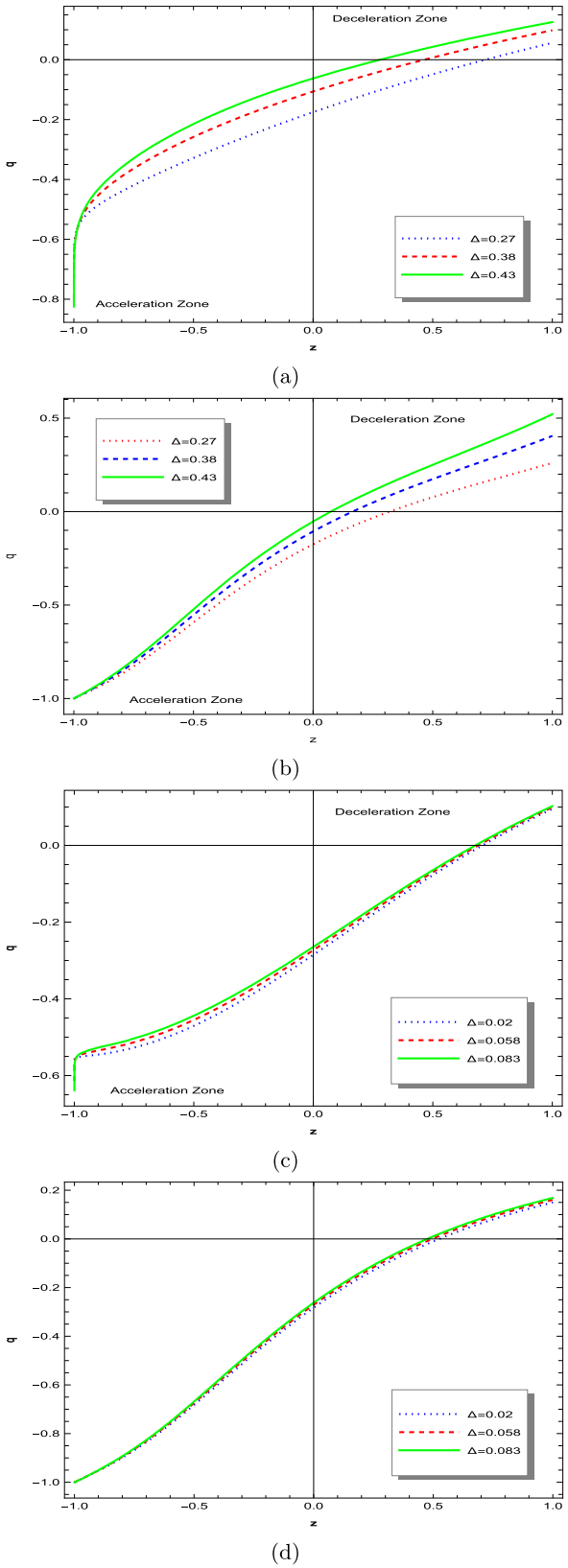

Fig. 6 Variation of the deceleration parameter q with redshift z: subfigures display the behavior of $q(z)$ for three values of Δ under four distinct scenarios: (**a**) BADE, (**b**) NBADE, (**c**) BADEI, (**d**) NBADEI

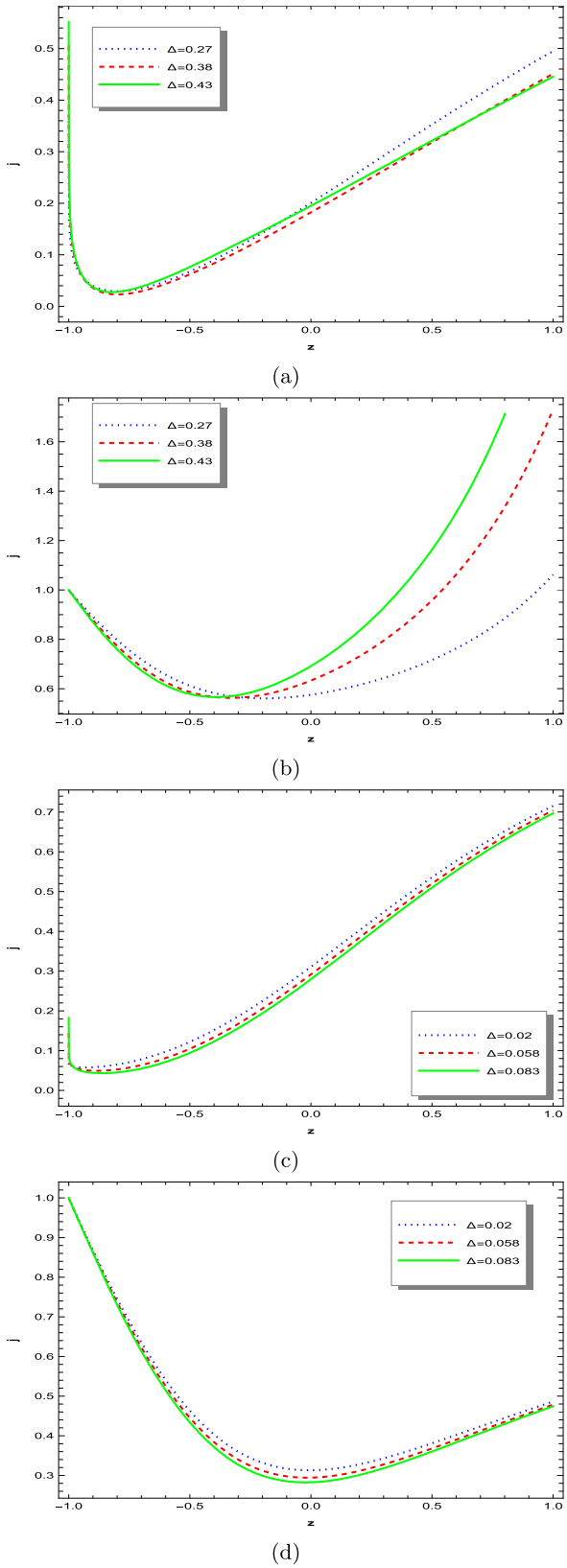

Fig. 7 Variation of the jerk parameter j with redshift z: subfigures display the behavior of $j(z)$ for three values of Δ under four distinct scenarios: (**a**) BADE, (**b**) NBADE, (**c**) BADEI, (**d**) NBADEI

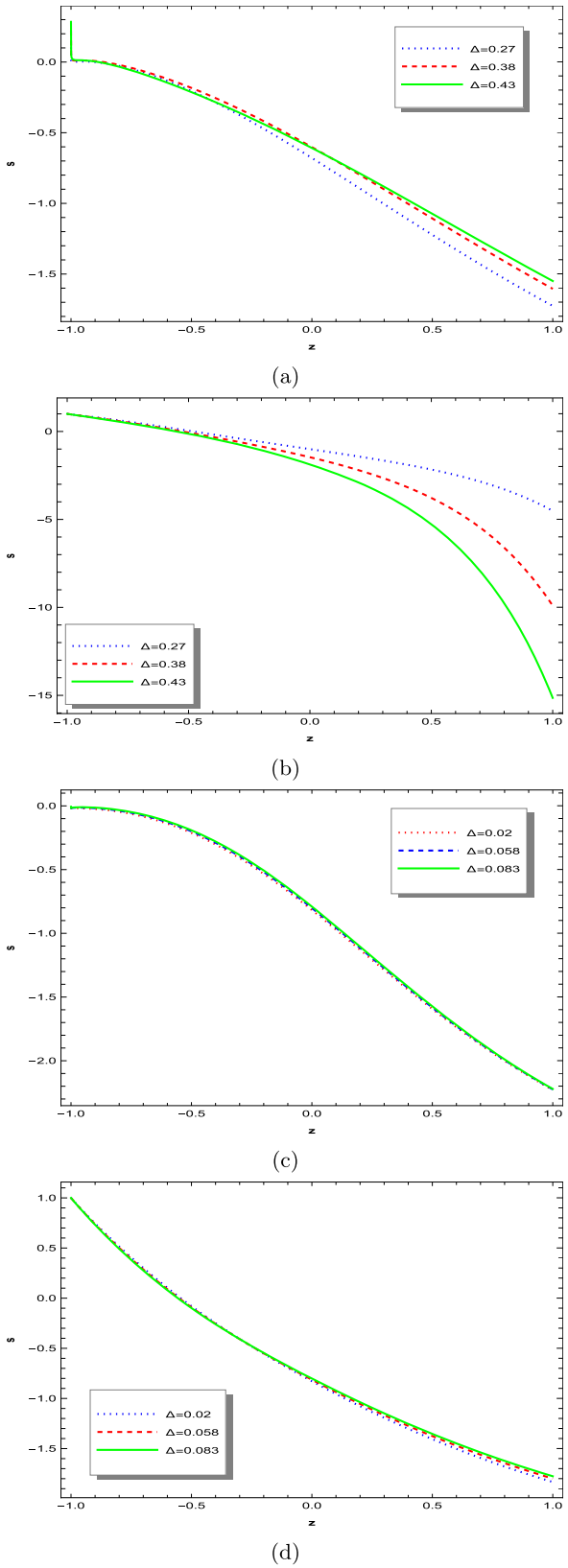

Fig. 8 Variation of the snap parameter s with redshift z: subfigures display the behavior of $s(z)$ for three values of Δ under four distinct scenarios: (**a**) BADE, (**b**) NBADE, (**c**) BADEI, (**d**) NBADEI

Three trajectories in the $q - S$ plane are shown in Fig. 10. For both the interacting and non-interacting cases, the three graphs begin in the region $q > 0$, which represents the deceleration zone, move through the region $q < 0$, which represents the acceleration zone, and ultimately arrive at the stationary position ($q = -1$, $S = 0$) for the NBADE model; however, the BADE model does not reach this fixed point.

Figure 11 displays the trajectories of evolution in the ω_d and ω_d' phase plane. The $\omega_d - \omega_d'$ plane, introduced by Caldwell and Linder [101], serves as a valuable tool for distinguishing between different dark energy models, where the prime denotes the derivative with respect to log a. Initially, the $\omega_d - \omega_d'$ plane was applied to the quintessence model, revealing two distinct regions: the thawing ($\omega_d < 0, \omega_d' > 0$) and freezing domains ($\omega_d < 0, \omega_d' < 0$). It was later generalized and extended to other dynamical dark energy models, as discussed in [102,103]. The paths defined in the NBADE model reach the ΛCDM fixed point ($\omega_d = -1, \omega_d' = 0$) in the later universe, traveling via the thawing zone ($\omega_d < 0, \omega_d' > 0$) in the interactive case and the freezing region ($\omega_d < 0, \omega_d' < 0$) in the non-interacting case. The trajectory paths of the BADE and BADEI models, however, traverse from the thawing to the freezing regions without achieving the ΛCDM fixed point. Since more acceleration is indicated by a freezing zone, the trajectories indicate the universe's present epoch. The same outcome is presented in [104] for BHDE in teleparallel gravity, while the reverse occurs in Tsallis HDE in the KS Universe [105].

8.2 Thermal stability

Finally, we have evaluated the thermal stability of our models by incorporating analyses of compressibilities and heat capacities. Applying the laws of thermodynamics to dark energy (DE) fluid theories can aid in constraining or even ruling out certain DE models. As observed from the trajectories illustrated in Fig. 12, both models in the interacting and non-interacting scenarios fail to meet the thermal stability criteria. This result aligns with the findings in the case of Tsallis holographic dark energy by [63] and, more broadly, with the conclusions of [61], which revealed that dark energy fluids with a time-dependent equation of state (EoS) parameter violate the physical constraints of thermodynamics. In reference [106], however, the author examined the Chevallier–Polarski–Linder model, generalized Chaplygin gas, and modified Chaplygin gas as dark energy components and showed that they exhibit thermal stability under some constraints on the model parameter. In [62], the authors derived constraints on the equation of state (EoS) parameter and the interaction term Q to determine the conditions under which a dark energy (DE) model achieves thermal stability. Their analysis showed that both positive and negative values of Q support thermal stability, and dark fluids with

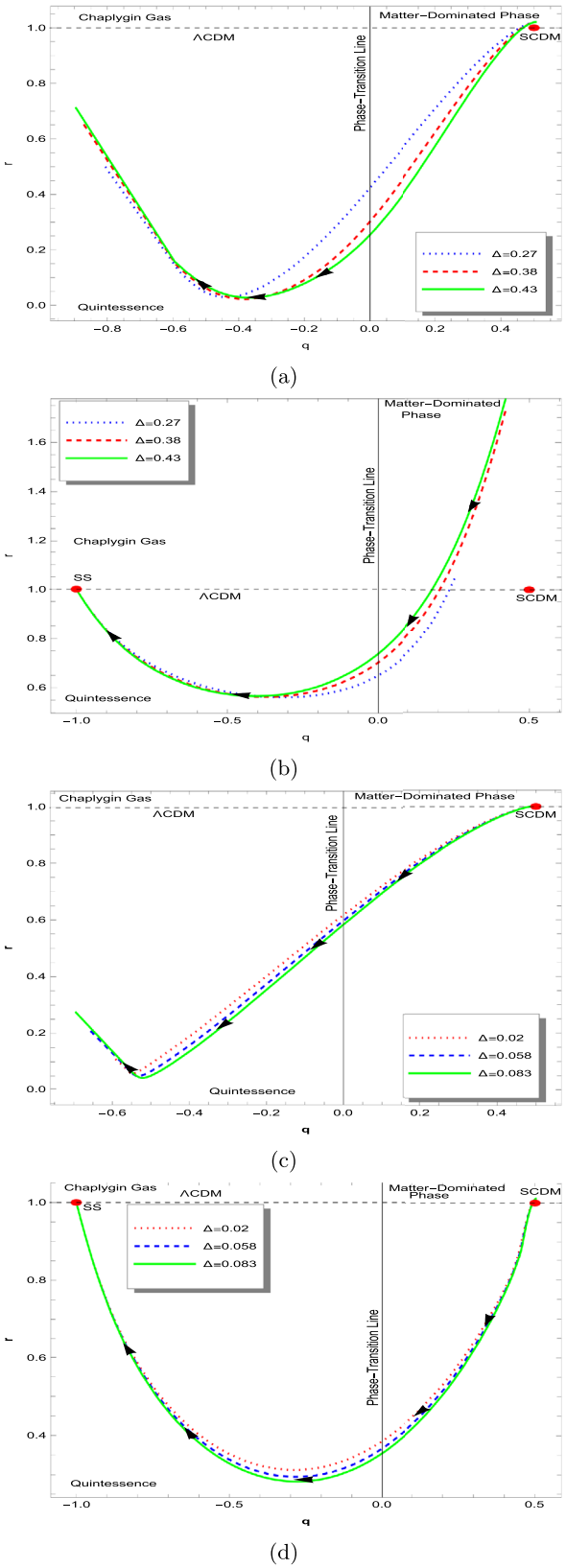

Fig. 9 Statefinder diagnosis in the $q - r$ plane: subfigures illustrate the trajectories of the cosmological models for three values of Δ under four distinct scenarios: (**a**) BADE, (**b**) NBADE, (**c**) BADEI, (**d**) NBADEI

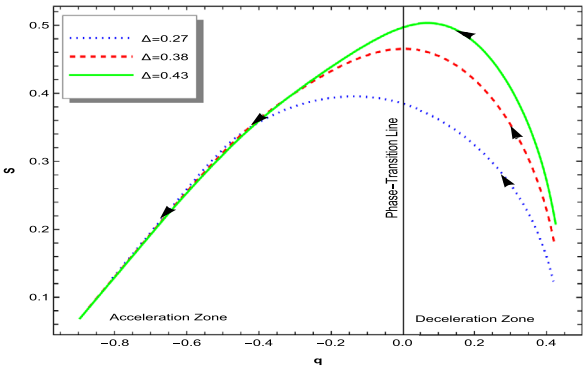

(a)

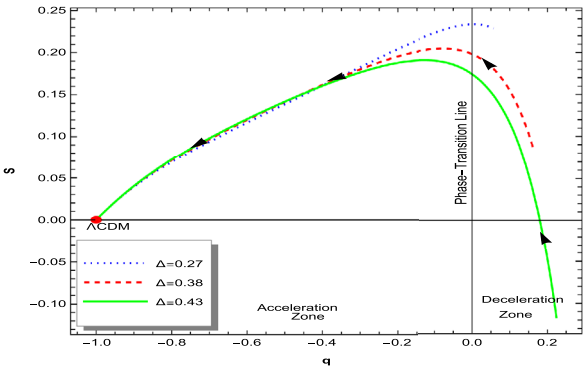

(b)

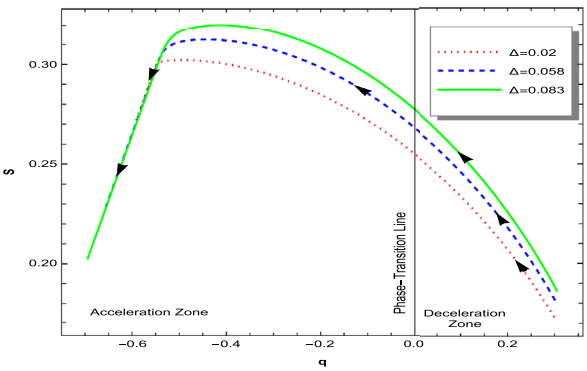

(c)

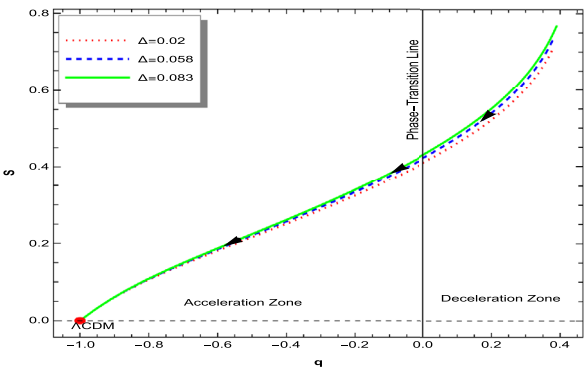

(d)

Fig. 10 Statefinder diagnosis in the $q - S$ plane: subfigures illustrate the trajectories of the cosmological models for three values of Δ under four distinct scenarios: (**a**) BADE, (**b**) NBADE, (**c**) BADEI, (**d**) NBADEI

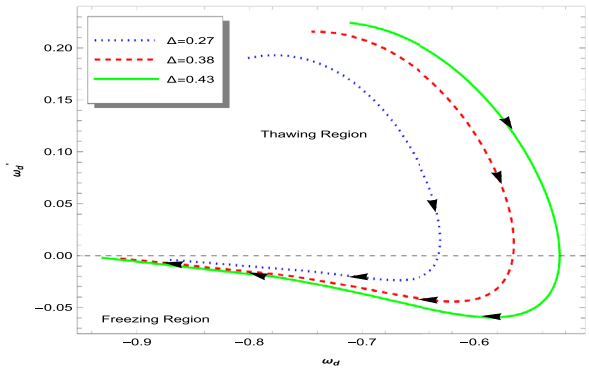

(a)

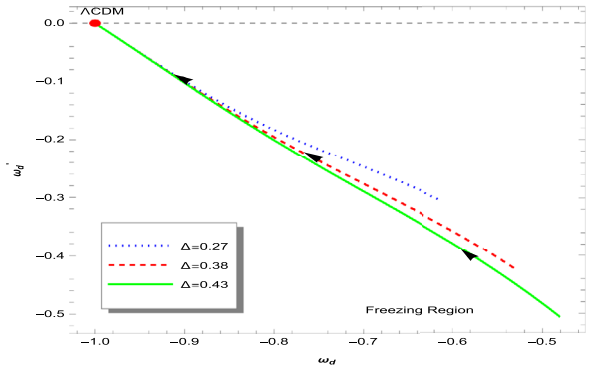

(b)

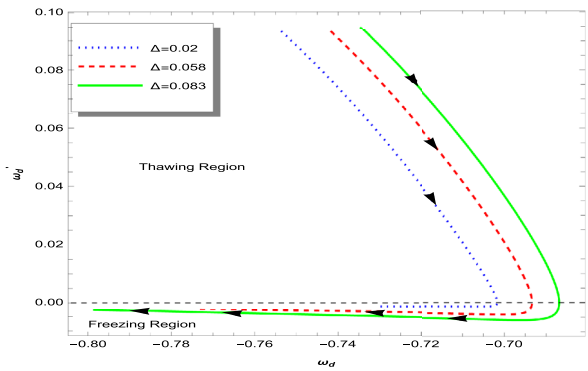

(c)

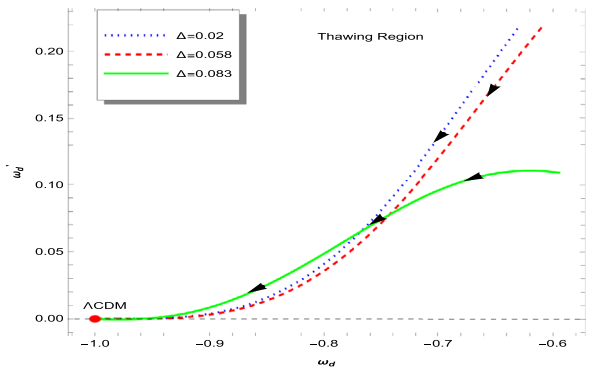

(d)

Fig. 11 Phase space analysis in the $\omega - \omega'$ plane: subfigures illustrate the trajectories of the cosmological models for three values of Δ under four distinct scenarios: (**a**) BADE, (**b**) NBADE, (**c**) BADEI, (**d**) NBADEI

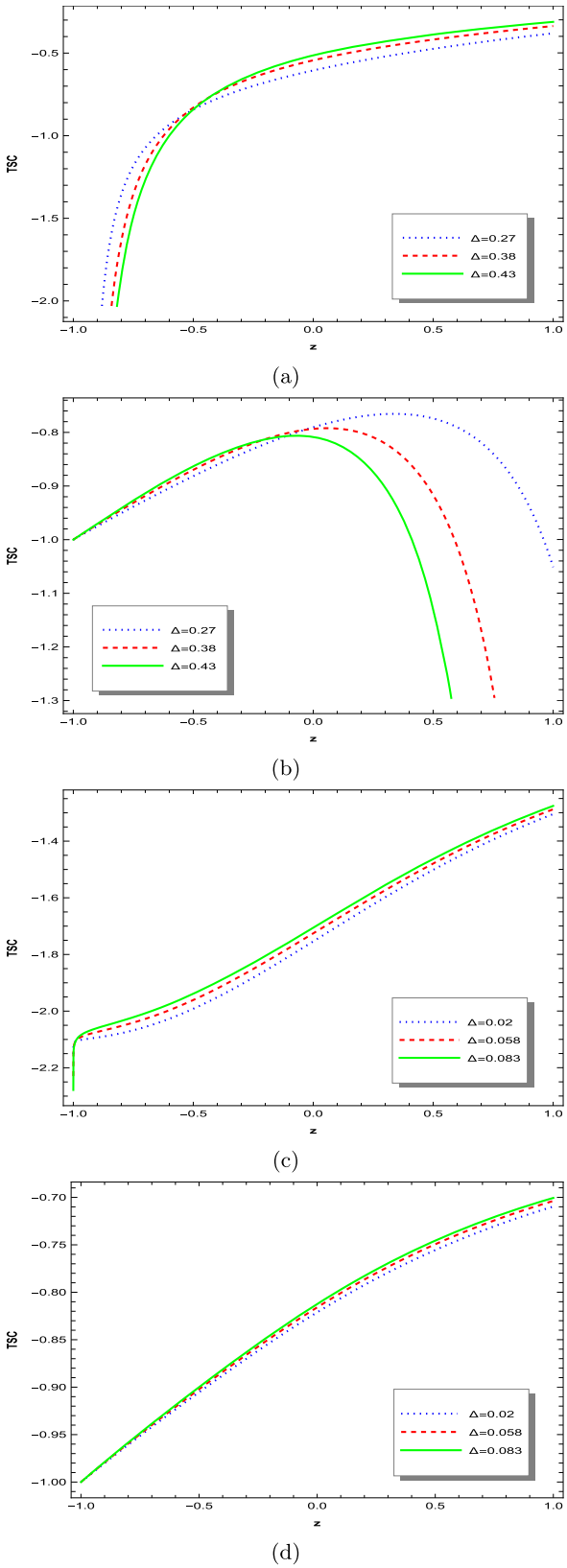

Fig. 12 Thermal stability analysis w.r.t. redshift z: subfigures illustrate the trajectories for three values of Δ under four distinct scenarios: (**a**) BADE, (**b**) NBADE, (**c**) BADEI, (**d**) NBADEI

an effective EoS parameter ($\omega_d > -1$) are thermodynamically stable. However, DE fluids exhibiting phantom behavior ($\omega_d < -1$) were found to be thermodynamically unstable, highlighting the thermodynamic challenges of phantom DE models.Although the EoS parameter for DE in our model lies within the range ($\omega_d > -1$), our analysis still indicates instability. A similar issue was reported in [64] for both interacting and non-interacting BHDE models.

Since our framework offers an initial approach to studying the influence of quantum gravity on the cosmic evolution of the Universe, future work will focus on exploring whether thermal stability for BADE and NBADE can be achieved by considering different IR cutoffs and/or generalized interactions between the dark sectors of the cosmos. Additionally, since our framework represents a preliminary attempt to explore how quantum gravity shapes the Universe's evolutionary timeline, it is important to analyze its consistency with the predictions of more fundamental quantum gravity theories.

8.3 Swampland conjecture

To understand the nature of DE, we have assumed that the scalar field ϕ is the sole source of energy, acting as the quintessence model. Figures 13 and 14 illustrates the behavior of our scalar field and potential with respect to redshift z. It is observed that the field increases with z and becomes finite at high redshift, with the exception of NBADEI, where the field demonstrates a steep increase at higher redshifts., suggesting a decrease as the Universe expands. Although the scalar field decreases in all cases, the characteristic feature of $\phi(z)$ being zero at the future infinity, where $\phi(z)\big|_{z=-1} = 0$, is exhibited only in the NBADEI model.It is evident that $|\phi(z)|$ is of order 1 in this model within the dark energy-dominated region, from $z \to -1$. Therefore, the swampland conjecture related to the scalar field is specially satisfied in the present universe for the NBADEI case. All the potentials are noticeably steeper in the early epoch, gradually flattening near the present time, specially for the BADE model in both interacting and non-interacting cases $v(\phi) \to 0$ as $z \to -1$.As a result, the quintessence field descends the potential more slowly as the Universe evolves.

To test the swampland conjecture for our models, we have plotted the constants C_1 and C_2 against the redshift z in Figs. 15 and 16. We can see from the graphs of C_1 that, with the exception of NBADE, C_1 does not disappear at future infinity. Notably, the value of C_1 is currently slightly greater than 1 in every instance except the BADEI example, and it gradually drops as z goes to -1. An analogous behavior is seen in the case of C_2, where it decreases and tends toward a non-zero finite value for each model in the distant future. Presently, when $z = 0$, the C_2 graph for every model, aside from BADEI, lies above 1, i.e., $C_1(0), C_2(0) \sim O(1)$. Refer-

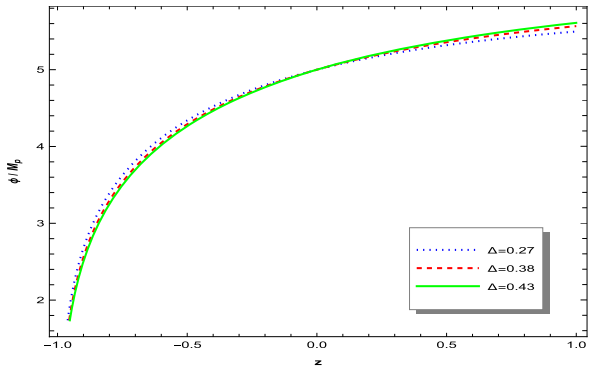

(a)

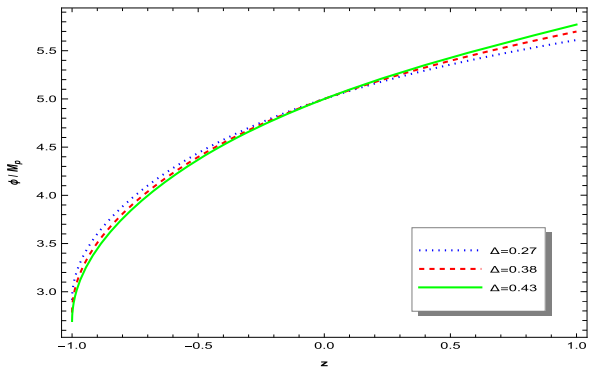

(b)

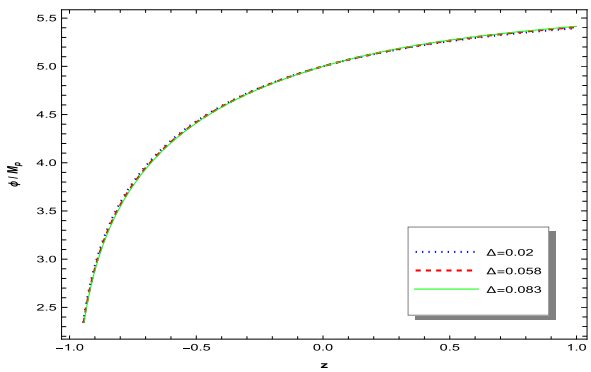

(c)

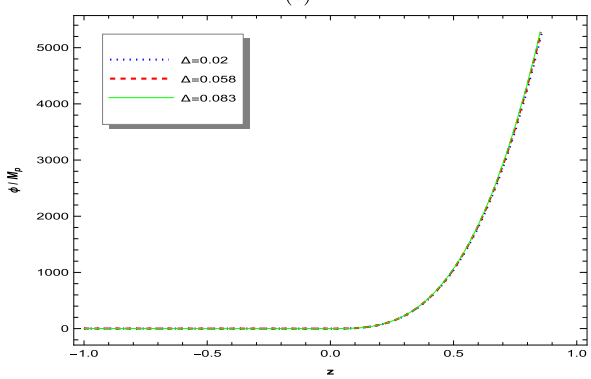

(d)

Fig. 13 Evaluation of scaler field ϕ with redshift z: subfigure depicts the variation of ϕ as a function of z under four distinct scenarios: (**a**) BADE, (**b**) NBADE, (**c**) BADEI, (**d**) NBADEI

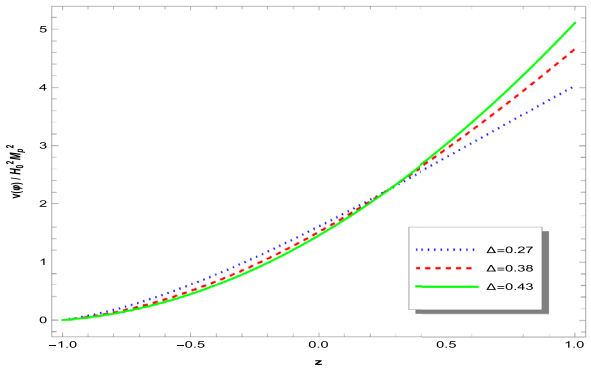

(a)

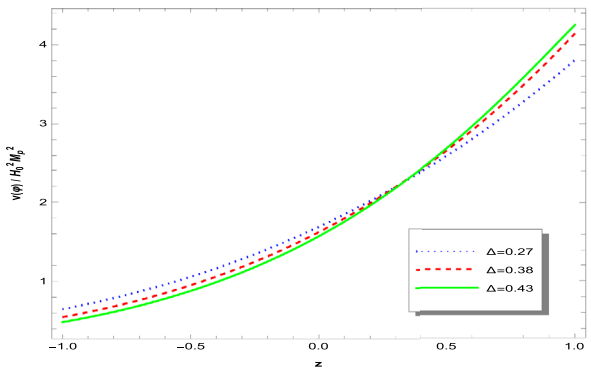

(b)

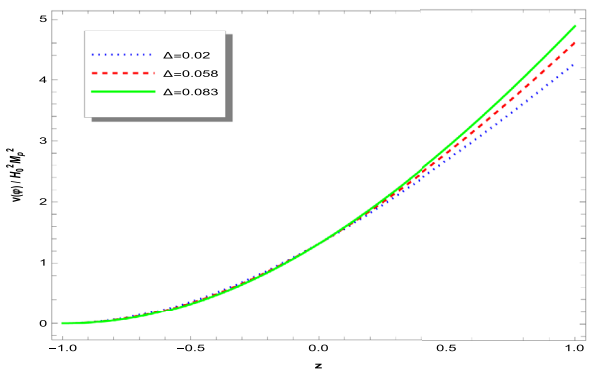

(c)

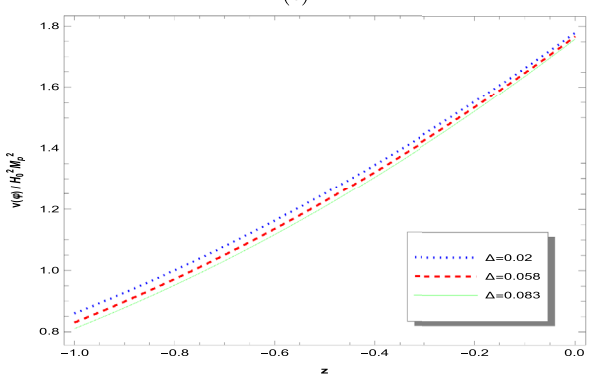

(d)

Fig. 14 Evaluation of scaler potential $v(\phi)$ with redshift z: subfigure depicts the variation of the relevant quantity as a function of z under four distinct scenarios: (**a**) BADE, (**b**) NBADE, (**c**) BADEI, (**d**) NBADEI [H_0 is in units of km/s/Mpc]

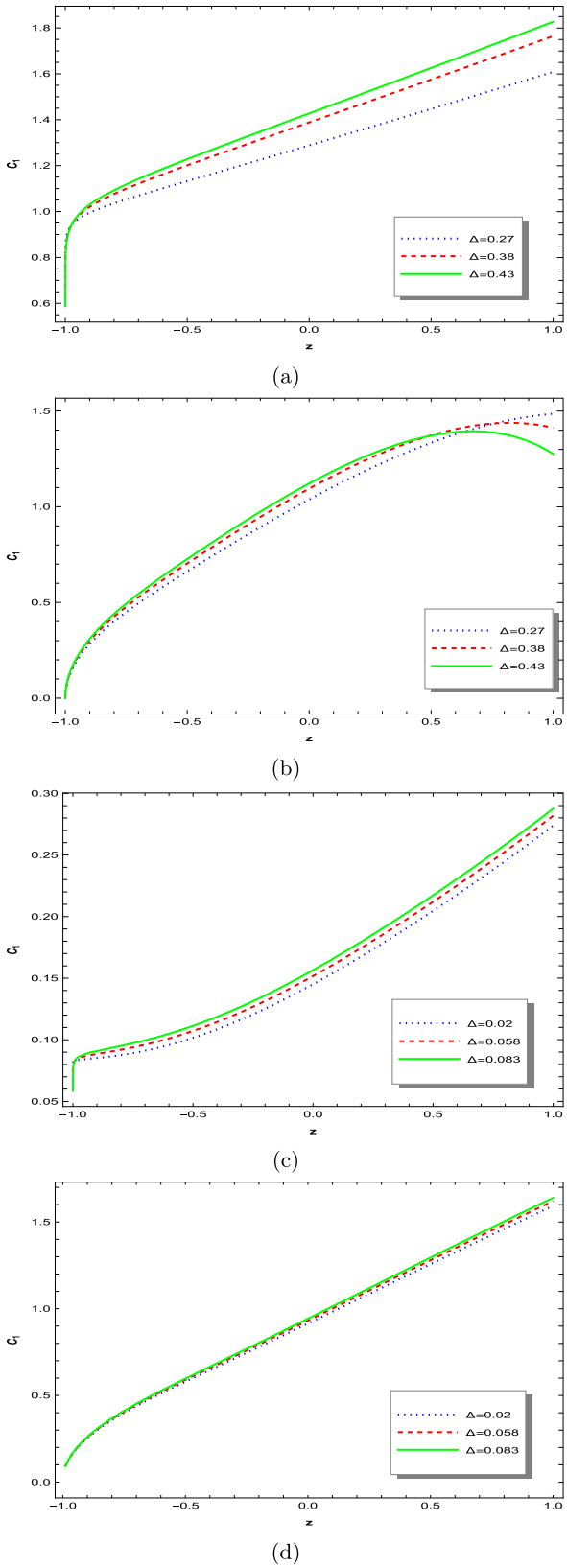

Fig. 15 Evaluation of swampland conjecture 1 with redshift z: subfigure depicts the variation of the relevant quantity as a function of z under four distinct scenarios: (**a**) BADE, (**b**) NBADE, (**c**) BADEI, (**d**) NBADEI

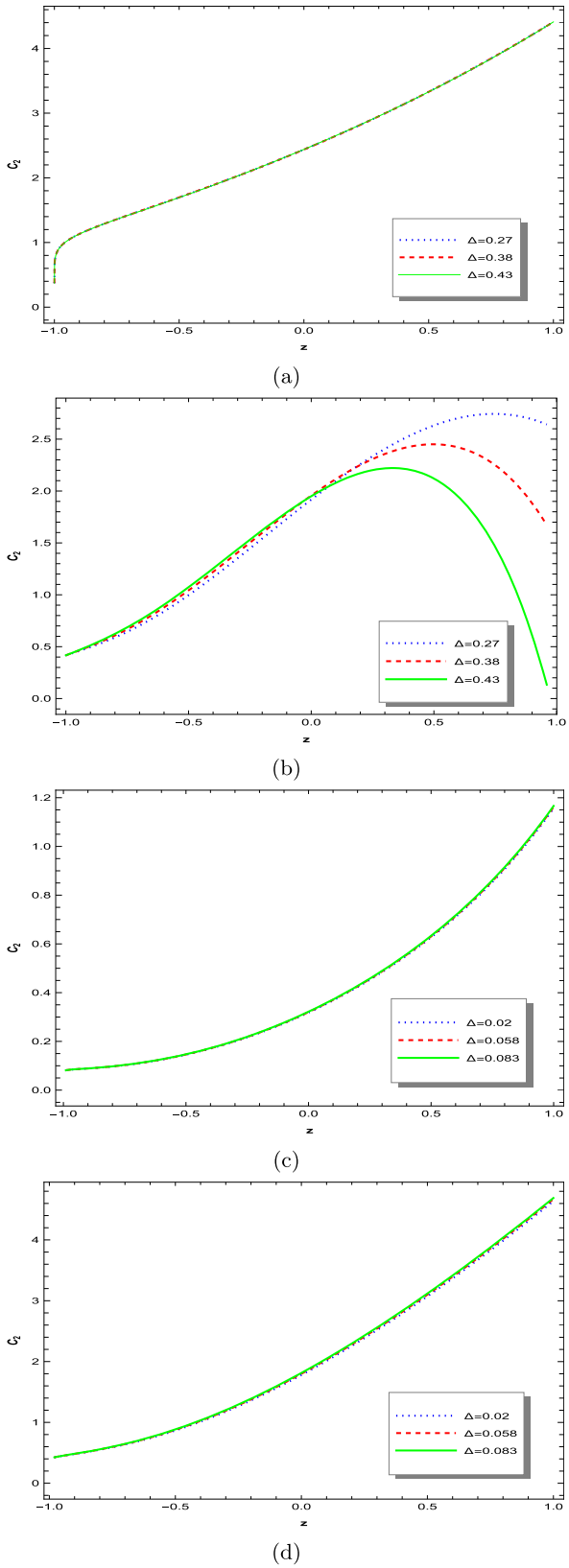

Fig. 16 Evaluation of Swampland Conjecture 2 w.r.t Redshift z: Subfigure depicts the variation of the relevant quantity as a function of z under four distinct scenarios: (**a**) BADE, (**b**) NBADE, (**c**) BADEI, (**d**) NBADEI

ence [107] has results of the same kind. The observation that C_1 and C_2 stay just above 1 for most models at $z = 0$ suggests that these models adhere to the bounds of the conjecture in the current epoch, but there is a tension with the conjecture at future infinity [108]. The BADEI model stands out with behavior that differs from the other models, particularly in the values of C_1 and C_2. This could suggest that additional constraints or modifications are needed for this model to fully align with the conjecture. The swampland conjectures show inconsistencies with the ΛCDM model and single-field slow-roll inflation. While it is not critical for our models to violate these conjectures, it would be ideal if the models we explored could still satisfy them, as the conjectures are intended to apply to the UV completion of effective field theories. For future studies, the swampland conjectures can guide the exploration of reconstructing the effective potential for multi-scalar fields rather than the single-scalar field we used, offering a possible approach for our model to satisfy the conditions.

8.4 Energy conditions

Energy conditions (ECs) are fundamental criteria in classical general relativity (GR) that describe the behavior of geodesics, including null, spacelike, timelike, and lightlike paths [109,110]. These conditions are essential for understanding the properties of cosmic geometries and the constraints imposed on the stress–energy–momentum tensor to ensure positive energy density. They play a significant role in analyzing spacetime singularities and determining the Universe's accelerating expansion phase in certain contexts [111,112]. The interaction type in interacting theories is also governed by ECs. For instance, the weak energy condition (WEC) is crucial for maintaining positive energy densities in matter, which ensures stability. Violations of ECs in interaction theories might hint at physics beyond the standard model. The four primary energy conditions are the weak energy condition (WEC), strong energy condition (SEC), dominant energy condition (DEC), and null energy condition (NEC), defined as follows for a perfect fluid:

- NEC : $\rho_{tot} + p_{tot} \geq 0$.
- WEC : $\rho_{tot} \geq 0$, $\rho_{tot} + p_{tot} \geq 0$.
- SEC : $\rho_{tot} + 3p_{tot} \geq 0$.
- DEC : $\rho_{tot} - |p_{tot}| \geq 0$.

Among these, the NEC is critical as its violation implies that none of the other energy conditions can hold. While other ECs may be violated by adjusting the cosmological constant (positive or negative) in realistic scenarios, breaching the NEC leads to catastrophic instability and indicates the presence of a ghost [113]. Since the NEC is typically satisfied in stable systems, it serves as a benchmark for analyzing various energy conditions. To evaluate the energy conditions in our model, we analyzed the NEC, SEC, and DEC through graphical representations.

On cosmological scales, the strong energy condition (SEC) must be broken [114], according to recent findings of the speeding Universe (Fig. 17). Since WEC → NEC, SEC → NEC, and DEC → NEC are the relationships between these energy conditions, the violation of the NEC suggests that none of the other energy conditions can be met [115]. We looked at the acceptable ranges for redshift z and the model parameter Δ, as shown in Fig. 18, in light of the importance of the SEC. According to our analysis, z varies between -1 to 0.3, and Δ varies between 0 to 1. The SEC's behavior is greatly impacted by these changes in z and Δ. In particular, the SEC shows some positive behavior for $z > 0.5$. However, the parameter range where the SEC violation is most noticeable was our main area of interest. As a result, the SEC has been broken. Additionally, Figs. 17 and 19 show that the NEC and DEC are complying.These behaviors are observed for each of the BADE, BADEI, NBADE, and NBADEI models.

9 Linear perturbation

In this section, we examine the impact of linear homogeneity and isotropic perturbations on the stability of the BADE and NBADE dark energy models in a non-flat universe. In order to evaluate how perturbations change under various physical circumstances, we take into account both interacting and non-interacting scenarios. Specifically, we introduce small deviations from the Hubble parameter, as given in Eq. (62), and the energy density evolution described in Eq. (63), to explore the dynamical behavior and robustness of the models [116].

Linear perturbation analysis plays a crucial role in cosmology, as it provides insights into the growth of structures and the evolution of density fluctuations. To further examine the structure formation aspect of these models, we study the growth rate f and the growth index γ, which provide a deeper understanding of how density perturbations evolve in the presence of dark energy. Additionally, we compare our theoretical predictions with observational constraints by plotting the evolution of $f\sigma_8$ data, an important observational probe for testing deviations from the standard ΛCDM model. While our models are consistent with the late-time accelerated expansion of the universe, it is essential to assess their ability to describe structure formation, which is a key challenge for any alternative to ΛCDM. By studying the behavior of perturbations in both interacting and non-interacting cases, we aim to determine whether these models offer distinctive features that could explain cosmic structure formation in a non-flat universe. This analysis reinforces the phenomeno-

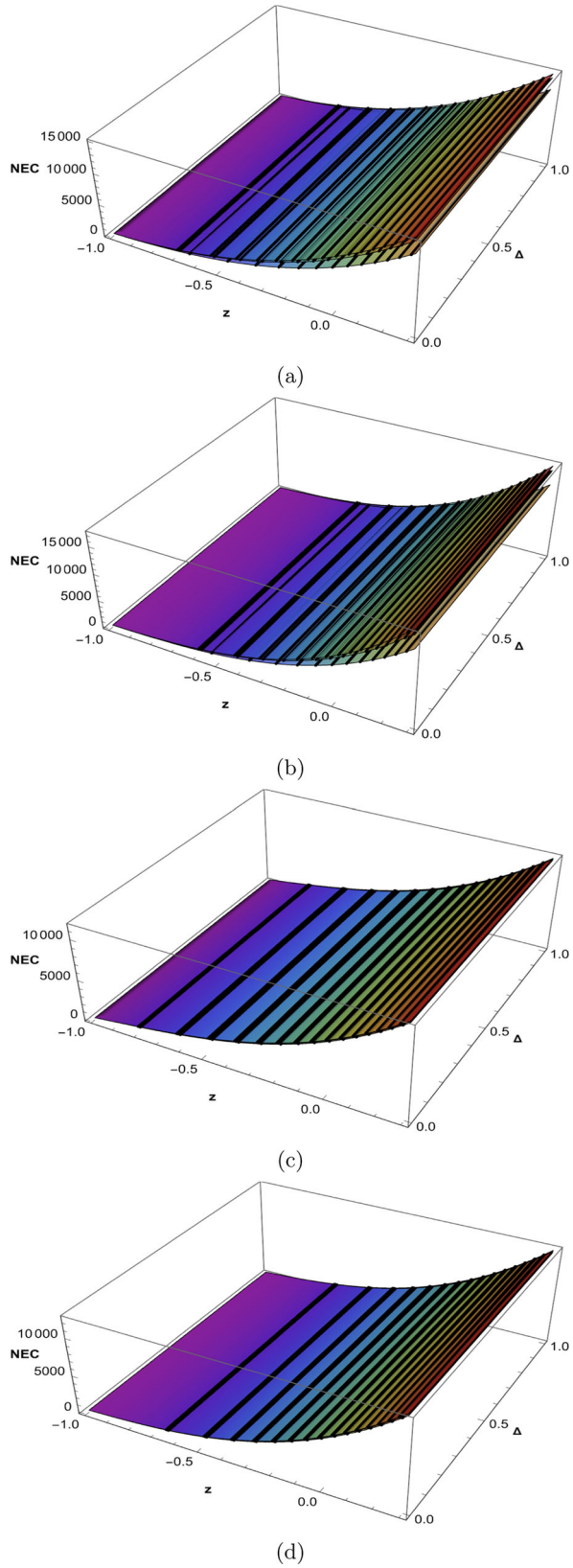

Fig. 17 3D plot of NEC w.r.t redshift z and Δ: subfigure depicts the variation of the relevant quantity as a function of z under four distinct scenarios: (**a**) BADE, (**b**) NBADE, (**c**) BADEI, (**d**) NBADEI

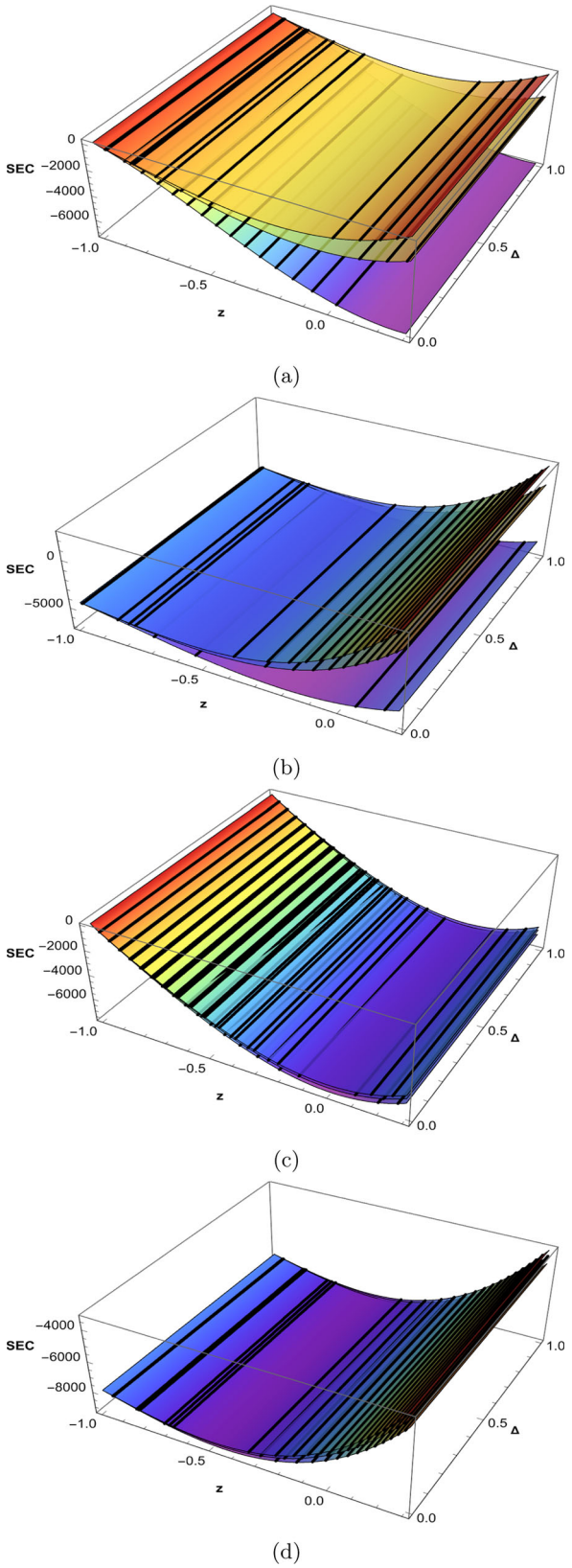

Fig. 18 3D plot of SEC w.r.t redshift z and Δ: subfigure depicts the variation of the relevant quantity as a function of z under four distinct scenarios: (**a**) BADE, (**b**) NBADE, (**c**) BADEI, (**d**) NBADEI

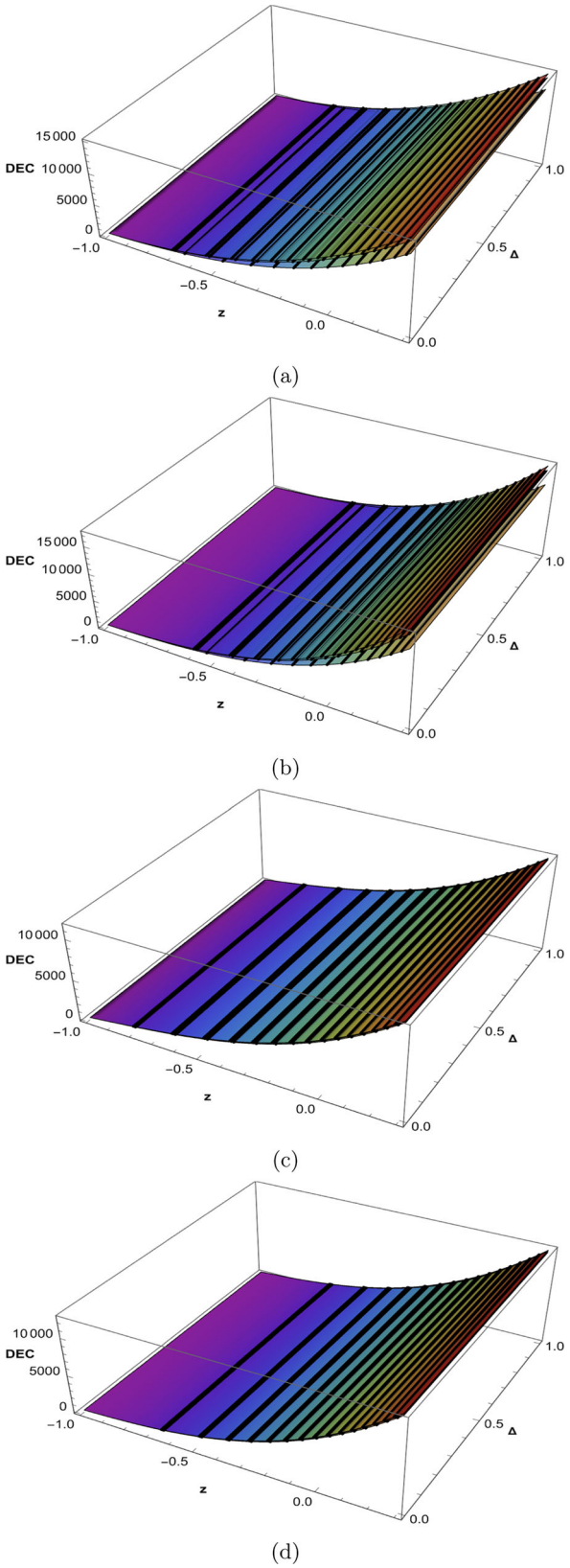

Fig. 19 3D plot of DEC w.r.t redshift z and Δ: subfigure depicts the variation of the relevant quantity as a function of z under four distinct scenarios: (**a**) BADE, (**b**) NBADE, (**c**) BADEI, (**d**) NBADEI

logical significance of BADE and NBADE models, ensuring that they are not only observationally viable but also theoretically robust in describing the evolution of cosmic structures.

The first-order perturbations that are being examined in this study are

$$\hat{H}(t) = H(t)(1 + \delta(t)) \tag{62}$$

$$\hat{\rho}_m(t) = \rho_m(t)(1 + \delta_m(t)), \tag{63}$$

where δ is the background Hubble parameter's isotropic deviation and δ_m is the matter overdensity. The Hubble parameter, ignoring the higher power of δ, can be written as

$$\hat{H}^2 = H^2(1 + \delta(t))^2 = H^2(1 + 2\delta(t)) \tag{64}$$

By substituting the perturbed Eq. (64) into the field Eq. (8), we obtain

$$\delta = \frac{\rho_m \delta_m}{6H^2} \tag{65}$$

Now using the continuity Eq. (13) we can get
For non-interacting case:

$$\dot{\delta}_m = -3H\delta(1 + \delta_m) \tag{66}$$

For interacting case:

$$\dot{\delta}_m = -3H\delta(1 + \delta_m)(1 - f^2) - 3f^2H(\delta_m - \delta)\frac{\Omega_d}{\Omega_m} \tag{67}$$

Now taking into account the Eqs. (66) or (67) and the relevant equations of $\dot{H}$ and $\dot{\Omega}_d$ we can solve numerically δ_m and δ(Here we take $\delta_m[0] = 1$ and the initial conditions for H and Ω_d are same as above).

The history of the perturbation terms $\delta_m(z)$ and $\delta(z)$ in terms of red-shift z is displayed in Figs. 20 and 21. For every illustration, the perturbations $\delta_m(z)$ and $\delta(z)$ both rapidly decrease. Notably, $\delta(z)$ approaches zero at late times for all models, suggesting that the background Hubble parameter stabilizes in the far future. However, the behavior of $\delta_m(z)$ differs between the interacting and non-interacting cases. In the interacting scenario, $\delta_m(z)$ also vanishes at late times, while in the non-interacting case, it does not necessarily reach zero. This suggests that interaction plays a crucial role in suppressing matter overdensities, potentially affecting structure formation. The results imply that the interacting model may lead to a more stable cosmic evolution, distinguishing it observationally from the non-interacting counterpart.

To gain a clearer understanding of the evolution of matter perturbations, it is useful to introduce the growth rate f, which is approximately determined by Wang and Steinhardt [117]: $f(z) = \Omega_m^{\gamma}$ where γ is the growth index defined by [99]

$$\gamma = \frac{3}{5 - \frac{\omega}{1-\omega}} + \frac{3(1+\omega)(1-\frac{3}{2}\omega)}{125(1-\frac{6}{5}\omega)^3}(1 - \Omega_m(z)) \tag{68}$$

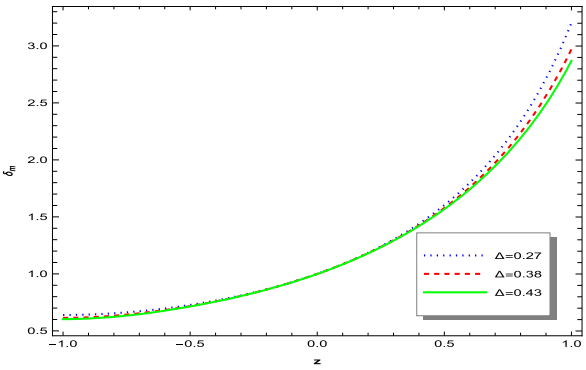

(a)

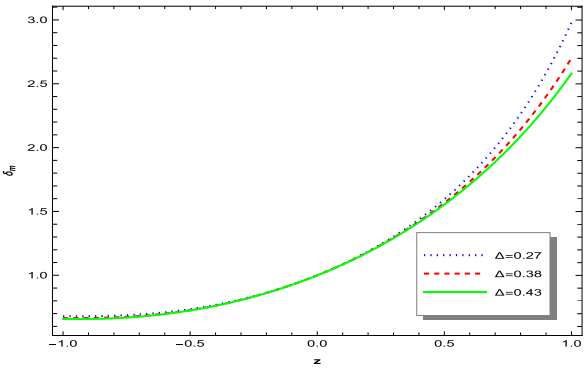

(b)

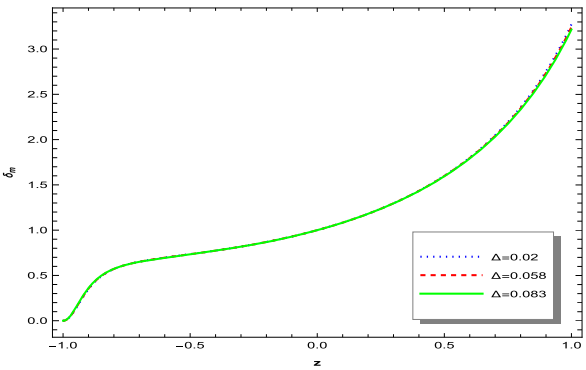

(c)

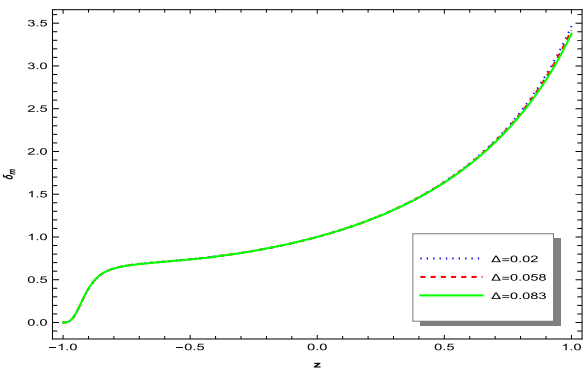

(d)

Fig. 20 Matter overdensity δ_m w.r.t redshift z: subfigure depicts the variation of the relevant quantity as a function of z under four distinct scenarios: (**a**) BADE, (**b**) NBADE, (**c**) BADEI, (**d**) NBADEI

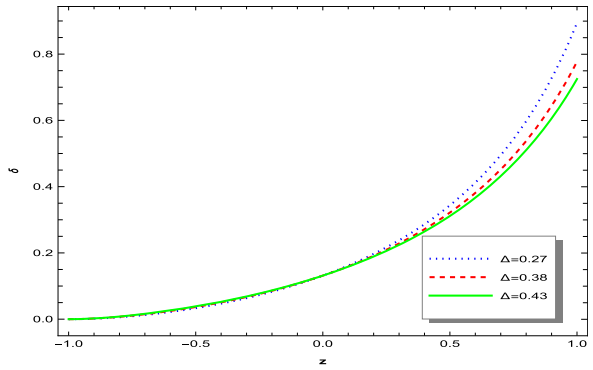

(a)

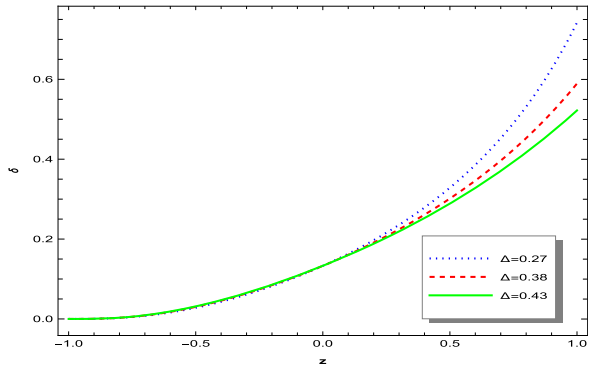

(b)

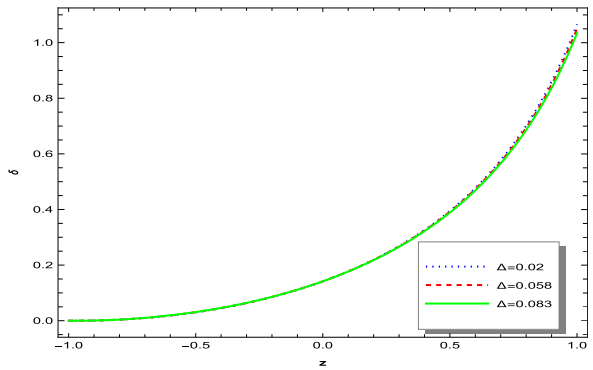

(c)

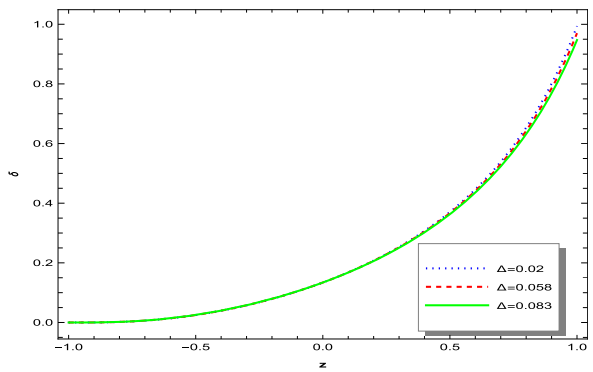

(d)

Fig. 21 Hubble parameter perturbation δ w.r.t redshift z: subfigure depicts the variation of the relevant quantity as a function of z under four distinct scenarios: (**a**) BADE, (**b**) NBADE, (**c**) BADEI, (**d**) NBADEI

where ω is the EoS parameter of the corresponding dark energy model.

The evolution of the growth index γ for each model is depicted in Fig. 22 , showing a decreasing trend over time. At present, the value of γ approaches near 0.55 for all cases, which is in good agreement with the standard ΛCDM model. The consistency of our results with previous studies suggests that the considered models provide a viable alternative to ΛCDM from the perspective of growth of structures [118].At present

The evolution of the growth rate f for each model is shown in Fig. 23, where we observe a decreasing trend as cosmic time progresses. At late times, f approaches zero, indicating the suppression of structure formation due to the dominance of dark energy. This behavior is in agreement with the standard cosmological model ΛCDM, where the growth rate decreases as the Universe transitions from a matter-dominated phase to an accelerated expansion phase [119]. The results further support the viability of our models in describing the evolution of large-scale structures.

In our analysis, we examine the evolution of the $f\sigma_8$ parameter, which serves as a crucial test for the growth of cosmic structures and provides a way to compare our model with observational data. The $f\sigma_8$ parameter is defined as:

$$f\sigma_8(z) = f(z)\cdot\sigma_8(z) = \frac{d\ln\delta_m}{d\ln a}\cdot\sigma_8(0)\frac{\delta_m(z)}{\delta_m(0)} \tag{69}$$

where $f(z) = \frac{d\ln\delta_m}{d\ln a}$ is the growth rate of structure and, $\sigma_8(z)$ is the rms amplitude of matter fluctuations on a scale of $8\,h^{-1}\,Mpc$. In our model, we adopt the present-day value $\sigma_8(0) = 0.811$, which is consistent with recent observational constraints. We use data points for $f\sigma_8$ from Reference [120] to plot and compare our model predictions with observations.

The resulting $f\sigma_8$ plot in Fig. 24 shows that our model's predictions align well with the observed data across a range of redshifts, suggesting that the growth rate of matter perturbations predicted by our models is in good agreement with current measurements. Among the different models considered, the NBADE model in the interacting case shows the best agreement with the observational data, suggesting that this scenario provides the most accurate description of the growth of cosmic structures. This consistency not only supports the validity of the BADE and NBADE models but also highlights their potential as viable alternatives to the standard ΛCDM framework in describing the late-time accelerated expansion of the universe.

10 Conclusions

In this study, we extend and enhance the analysis of the Barrow agegraphic dark energy (BADE) and new Barrow agegraphic dark energy (NBADE) models presented in Refs.

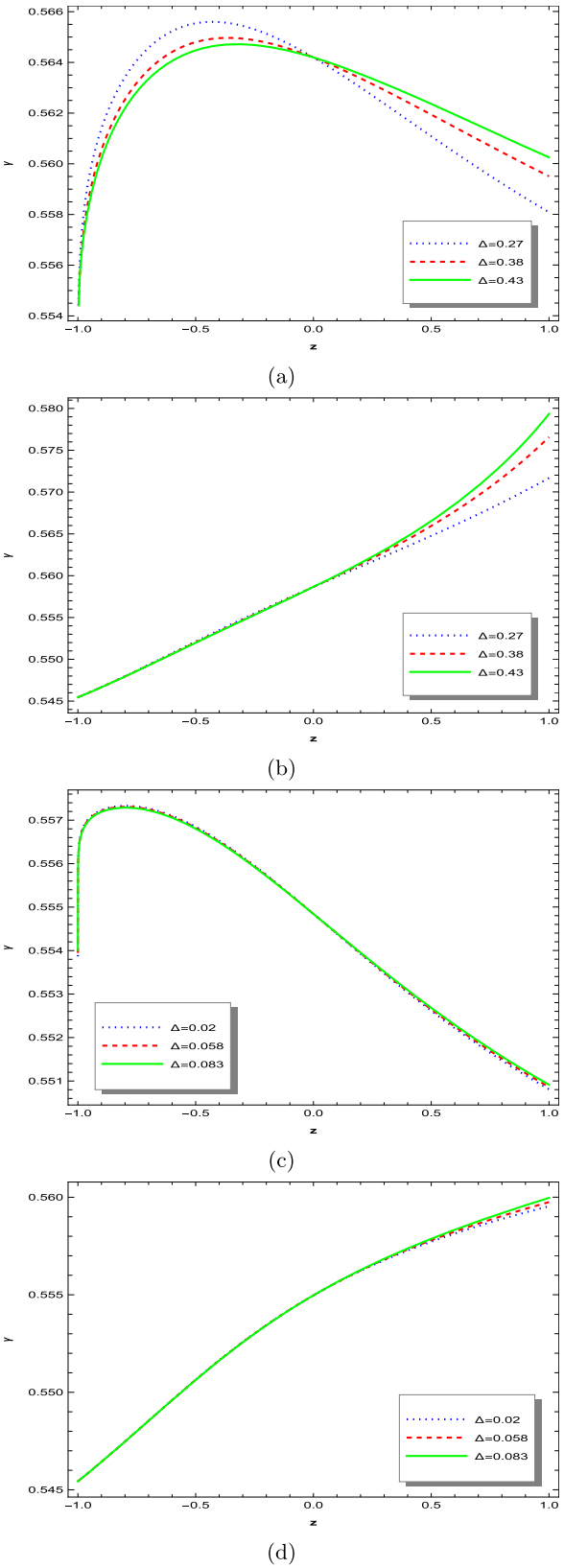

Fig. 22 Growth index γ w.r.t redshift z: subfigure depicts the variation of the relevant quantity as a function of z under four distinct scenarios: (**a**) BADE, (**b**) NBADE, (**c**) BADEI, (**d**) NBADEI

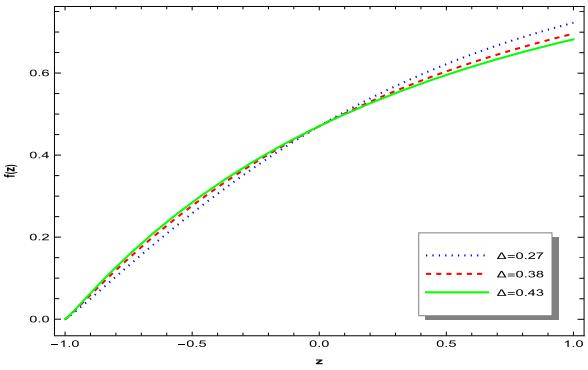

(a)

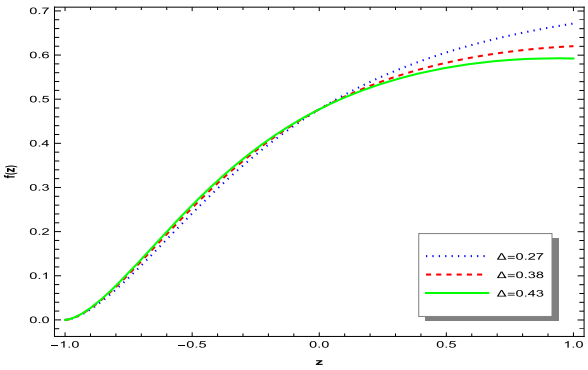

(b)

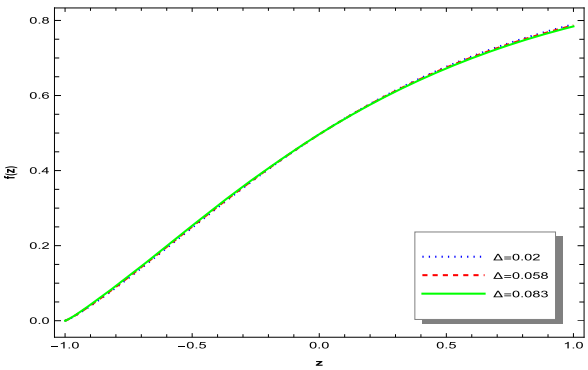

(c)

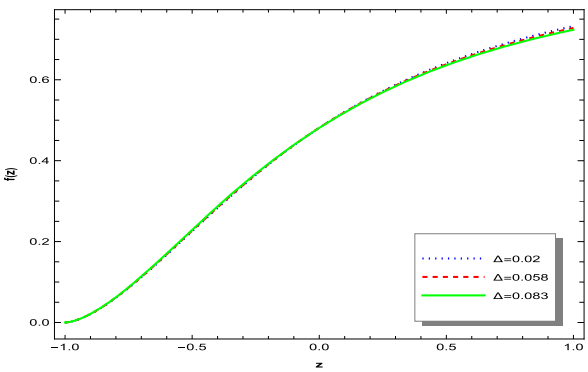

(d)

Fig. 23 Growth rate f w.r.t redshift z: subfigure depicts the variation of the relevant quantity as a function of z under four distinct scenarios: (**a**) BADE, (**b**) NBADE, (**c**) BADEI, (**d**) NBADEI

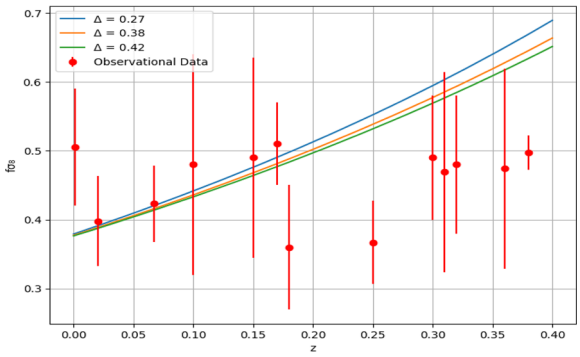

(a)

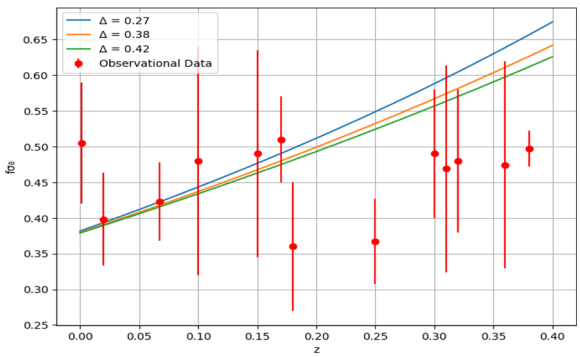

(b)

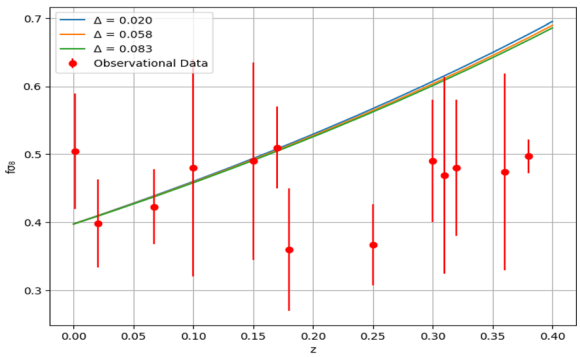

(c)

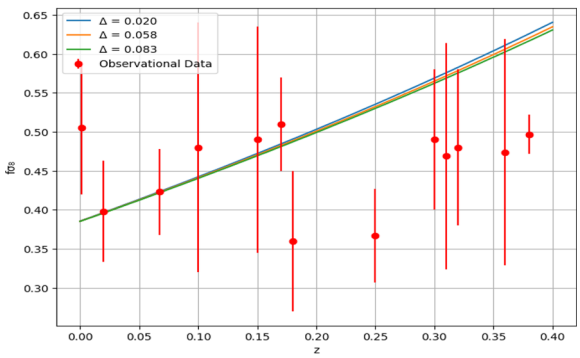

(d)

Fig. 24 Plot of growth rate $f\sigma_8$ w.r.t redshift z for growth rate data: (**a**) BADE, (**b**) NBADE, (**c**) BADEI, (**d**) NBADEI

[9,25]. Unlike these previous studies, which focused primarily on non-interacting scenarios in a flat universe, we investigate both interaction and non-interaction cases in a non-flat universe. This allows us to assess the impact of spatial curvature and the exchange of energy occurring between dark matter and dark energy more comprehensively. Additionally, we perform parameter estimation using baryon acoustic oscillation (BAO) data-an approach not adopted in Refs. [25,29] – to derive more precise constraints on the model parameters. Moreover, our work introduces several new analyses that were not considered in previous studies, including a detailed examination of thermal stability, an assessment of energy conditions (NEC, DEC, SEC), and an exploration of the Swampland Conjectures within the BADE and NBADE frameworks. The inclusion of the Swampland Conjectures is particularly novel, providing new insights into the compatibility of these models with quantum gravity constraints-an aspect that has not been explored before. Furthermore, we calculate the Akaike information criterion (AIC) and Bayesian information criterion (BIC) for our models to evaluate their statistical viability. Notably, the reduced chi-squared value for the BADE model is found to be lower than that of the ΛCDM model, suggesting that the BADE model may offer a more accurate agreement with the observational data. In addition to these analyses, we also perform a linear perturbation analysis to examine the growth of matter density perturbations and assess the stability of the models at the perturbative level. This analysis provides new insights into the evolution of cosmic structures under the influence of BADE and NBADE. By addressing these additional aspects, our work significantly expands upon the previous findings, offering a more detailed and robust examination of these dark energy models. By incorporating Barrow entropy and considering two IR cutoffs-universe age and conformal time-two novel dark energy models, namely Barrow agegraphic dark energy and new Barrow agegraphic dark energy, were proposed. This paper examines four scenarios: BADE and NBADE (non-interacting dark energy and dark matter) and BADEI and NBADEI (interacting dark energy and dark matter). During our investigation, we introduce an interaction term $Q = 3f^2H(\rho_d+\rho_m)$ to model the energy exchange between dark matter and dark energy. The choice of this form is motivated by several theoretical and observational considerations. First, this interaction ensures a self-consistent energy transfer that preserves the overall conservation of energy in the cosmic fluid. The presence of the Hubble parameter H naturally incorporates the effect of cosmic expansion, while the dependence on $\rho_d+\rho_m$ allows the energy exchange to evolve dynamically with the relative densities of dark matter and dark energy. We emphasize that the chosen ansatz for Q is not arbitrary; rather, it was specifically selected to ensure that the ratio of dark matter to dark energy densities approaches a fixed value at late times, thereby addressing the coincidence problem [121,122]. Additionally, this interaction form results in a constant but unstable ratio at early times. It is challenging to conceive of a simpler expression for Q that naturally incorporates these two essential properties. Furthermore, this formulation can be reinterpreted as implying an effective exponential potential for the quintessence field at late times, a well-established result previously derived by Zimdahl et al. [123]. Similarly, in [124], it was noted that the effective potential of the interacting quintessence model (IQM) exhibits a power-law dependence on the quintessence field during early times and transitions to an exponential dependence at late times. Furthermore, the presence of Q modifies the growth of cosmic structures. As shown in reference [125], interaction leads to slower growth of matter perturbations, which consequently modifies the shape of the matter power spectrum.

Furthermore, since our model parameters are constrained using observational data (e.g., cosmic chronometers, BAO), introducing a different interaction form would require a complete reanalysis, including parameter estimation and statistical validation. While there is no general consensus on the exact form of the interaction term, different functional forms, including nonlinear extensions, could be explored to assess their impact on late-time cosmic evolution. However, such modifications require a complete reanalysis of observational constraints, as they introduce additional degrees of freedom that affect key cosmological parameters. Given the current observational consistency of our model, we focus on this well-motivated form of Q, leaving the exploration of alternative interaction models that could reduce the observed deviations at higher redshifts while maintaining consistency with current observational constraints for future studies. A primary focus is placed on constraining the model parameters using observational data to ensure their compatibility with the universe's expansion history and dynamics. These constraints are crucial for understanding the models' implications on cosmological parameters, thermal stability, the swampland conjecture, and energy conditions, providing a comprehensive assessment of their physical validity and theoretical consistency. In order to achieve this, the CC+bao samples will fit the BADE and NBADE taking into account the noninteraction and linear interaction factors in order to examine the Hubble $H(z)$, dark-energy equation of state ω, and deceleration q parameters.

- Investigating the $H(z)$ parameter reveals that our models align well with observational data, demonstrating strong consistency with current measurements of the Hubble parameter. When comparing the $H(z)$ plot of our models with the standard ΛCDM model, we find a similar behavior, further supporting the validity of our models in describing the universe's expansion history. This comparison reinforces the potential of our mod-

els as accurate representations of cosmological dynamics, offering an alternative framework to the ΛCDM paradigm. In the interacting scenarios of the BADE and NBADE models, we find that the estimated value of H_0 is $H_0 = 69.9216662 \pm 0.80655578$ and $H_0 = 68.0013342 \pm 0.92303832$ which are higher and closer to those predicted by the ΛCDM model. This observation underscores the significance of considering the interaction between dark energy and dark matter. However, if we evaluate the models based on the Akaike information criterion (AIC) and Bayesian information criterion (BIC) values (presented in the Table 5), we find that in the non-interacting scenarios, the ΔAIC and ΔBIC values are smaller, making them more supportive of the ΛCDM model. This highlights the nuanced trade-offs between theoretical alignment and observational support, emphasizing the importance of exploring both scenarios in the quest to understand the dynamics of the universe.

- Following $H(z)$ analysis, we examine each model's EoS and deceleration parameters with respect to redshift z. The equation of state (EOS) parameter for each model lies in the quintessence-like era, with a notable feature of converging to the ΛCDM fixed point ($z = -1, \omega_d = -1$) in the distant future. This behavior is particularly achieved by the NBADE model, both in the interacting and non-interacting cases, indicating its tendency to approach the cosmological constant era as the universe evolves. The deceleration parameter, on the other hand, moves from the deceleration phase to the acceleration phase with consistent behavior across all models. Interestingly, in both the interacting and non-interacting instances, the NBADE model converges to the ΛCDM fixed point ($q = -1$) when z goes to -1, confirming the model's compatibility with the conventional cosmological framework in the far future.

To provide a comprehensive perspective, Table 6 below presents the values of the equation of state (EoS) parameter, deceleration parameter, and transition redshift at present, comparing the results from our models with observational constraints. Our models predict an equation of state (EoS) parameter ω_0 in the range $[-0.75, -0.64]$, which is slightly less negative than the observational constraints from Planck, WP, and BAO data. This discrepancy can be attributed to the unique features of the BHDE and NBADE models, particularly the fractal structure of spacetime encoded in the Barrow exponent Δ. The Barrow exponent Δ, which quantifies the deviation from standard entropy, might be influencing the EoS. A smaller Δ results in a minimal deviation from ΛCDM, while a larger Δ could push ω_0 toward less negative values. In the DE model, the use of conformal time or the age of the universe as a cutoff scale might lead to a different evolution of ω_0 compared to standard holographic

Table 6 Theoretical and observational values of EoS parameter, transition redshift, deceleration parameter in the current epoch

	BADE	BADEI	NBADE	NBADEI	Observational value
ω_0	[− 0.65345, − 0.525938]	[− 0.752196, − 0.72893]	[− 0.64021, − 0.53054]	[− 0.75046, − 0.724042]	[− 1.38, − 0.89] (Planck+WP+BAO) [126]
					[− 0.62, − 0.74] (SNIa+BAO/CMB) [127]
z_t	[0.26854, 0.72234]	[0.66550, 0.70044]	[0.07123, 0.32941]	[0.45851, 0.544578]	[0.5, 0.64] (SNIa+CMB) [128]
					[0.67, 0.77] (SNIa+BAO/CMB) [129]
q_0	[− 0.20847, − 0.06179]	[− 0.29489, − 0.26555]	[− 0.20647, − 0.057282]	[− 0.30453, − 0.25822]	[− 0.86, − 0.42] (Union2 SNIa) [96]

dark energy, causing it to be less negative. Additionally, our results show that the EoS parameter in the interaction case is more negative than in the non-interacting case. This suggests that the interaction between dark matter and dark energy can enhance the effective negative pressure, thereby strengthening the accelerated expansion. While this deviation from the referenced observation may seem significant, it is consistent with other dark energy models discussed in the literature. For instance, the authors [127] used the Union 2.1 and supernova datasets to assess the results of a cosmographic examination of the equation of state parameter using Padé approximations and found that the EoS parameter was constrained to lie within $[-0.74,-0.62]$, which aligns more closely with our findings. A study [130] using the BAO dataset found that for a flat CPL (Chevallier–Polarski–Linder) model, ω_0 ranges from $[-0.94, -0.28]$, and for a non-flat CPL model, it lies within $[-1.02, -0.10]$. This suggests that EoS parameterizations have little impact on deviations from ΛCDM and hints that dark energy may have dynamic properties. Using the DES-SN5YR sample, they found the strongest tension with ΛCDM at 3.9σ, with $\omega_0 = -0.727 \pm 0.067$ [131]. When combining DESI and SDSS BAO data and selecting the most precise BAO distance measurements in each redshift bin, they obtained $\omega_0 = -0.761 \pm 0.064$, showing a 3.5σ deviation from ΛCDM and closely aligning with the DES-SN5YR results [132]. Another study presenting ω_0 values that closely align with our model predictions can be found in [133,134]. The consistency across independent studies strengthens the case for a dynamical dark energy model.

The slight differences between our results and those of [126] could be due to the use of different datasets or methodologies. For example, [126] used a broader range of cosmological measurements, while our analysis focused on a more refined subset of BAO+CC data. Future work will focus on refining the model parameters and incorporating additional datasets to better constrain ω_0 and explore the implications of this deviation for the evolution of the universe. From an observational perspective, our analysis reveals that the interacting cases yield better agreement with observational data compared to the non-interacting scenarios. This suggests that incorporating interaction between dark energy and dark matter enhances the models'ability to describe the dynamics of the universe more accurately. Such behavior is further driven by the coupling parameter f, which governs the strength of interaction, offering deeper insights into the dynamical evolution of the universe and improving the models' consistency with cosmic observations.

- After analyzing the behavior of the Hubble parameter and the deceleration parameter, we proceed to examine the evolution of two important parameters: the jerk and snap. These higher-order parameters provide deeper insights into the dynamics of the universe's expansion, capturing the transition between different phases of cosmic acceleration and offering additional constraints on the viability of the models. Throughout the span of the universe's evolution, the jerk parameter stays positive, suggesting an ongoing acceleration. In particular, the NBADE model (in both interacting and non-interacting situations) exhibits constant acceleration comparable to the ΛCDM model in the distant future. For every model, the snap parameter's behavior demonstrates a phase shift from the negative to the positive zone and tends to 1 in the distant future for both interactive and non-interacting cases of the NBADE model, as z goes to -1.
- The evolution trajectories in the $q - r$ plane start from the SCDM point ($q = 0.5, r = 1$), transition through the deceleration to the acceleration zone for BADE, BADEI, and NBADEI, and remain in the quintessence zone without entering the Chaplygin region. The NBADE model begins in the matter-dominated phase but later follows the same path, ending at the de Sitter fixed point ($q = -1, r = 1$) for both interacting and non-interacting cases. In the $q - S$ plane, the trajectories for each model start in the deceleration zone ($q > 0$) and go into the acceleration zone ($q < 0$). One unique characteristic of the NBADE model is that the trajectories end at the ΛCDM fixed point ($q = -1, S = 0$) in both interacting and non-interacting situations.A key finding is that, in the interacting cases of both models, the trajectories in the $q - r$ plane pass through the SCDM fixed point, a feature that is not observed in the non-interacting scenarios. This behavior suggests that the interaction between dark energy and dark matter leads to a more consistent alignment with the standard cold dark matter (SCDM) model, which could have important implications for understanding the evolution of the universe.
- We analyzed by another diagnostic tool, the $\omega_d - \omega_d'$ analysis; most models show trajectories in the freezing region, indicating cosmic acceleration, while the interacting NBADE model lies in the thawing region, suggesting weaker acceleration.
- Thermal physics plays a crucial role in dark energy studies, as the laws of thermodynamics are universally applicable to macroscopic systems and grounded in experimental evidence. So in our study, we examined the thermal stability of our model using the parameter values obtained from parameter estimation using CC+Bao data and found it to be thermally unstable.Future research will concentrate on determining whether thermal stability for BADE and NBADE can be attained by taking into account various IR cutoffs and/or generalized interactions between the dark sectors of the universe, as our framework provides a preliminary method for examin-

ing quantum gravity effects on the cosmic history of the Universe.

- We also examine the recently proposed swampland criteria for the model, and the findings are intriguing.Notably, the potential $v(\phi)$ becomes asymptotically flat in the distant future ($z \to -1$). Furthermore, the parameters of the swampland criterion parameters C_1 and C_2 are of O(1) at present ($z = 0$) but approach a positive constant as $z \to -1$. Additionally, from a theoretical perspective, we find that the interacting NBADE model satisfies the Swampland Conjecture related to the scalar field, which further strengthens its viability in the context of string theory, as it respects the constraints placed on scalar fields in quantum gravity. Despite this result, we do not believe that our models are entirely confined to swampland. It is important to note that the model lacks an explicit scalar field and potential. The stress-energy tensor of the holographic fluid, from which the potential can be derived, is effective only at low energies. There remains a possibility to reconcile each model with the string landscape by invoking a phase transition in the universe, which lies beyond the scope of the low-energy effective behavior discussed here.
- Additionally, we investigated the energy conditions for our models, which provided valuable insights into their consistency with physical constraints and the stability of the universe's evolution. We looked into the three energy conditions-NEC, SEC, and DEC-we discovered that while the SEC is broken in every instance, the NEC and DEC are satisfied. We conclude that our models are stable since all stable systems satisfy the NEC. The current acceleration of the cosmos is further indicated by the violation of the SEC, which is consistent with cosmic expansion data.
- Next, we performed a detailed linear perturbation analysis to examine the evolution of matter density perturbations within the frameworks of the Barrow agegraphic dark energy (BADE) and new Barrow agegraphic dark energy (NBADE) models. The results show that the matter density contrast δ_m decreases with redshift and tends towards zero in the interacting case for both models, indicating a suppression of structure growth due to energy exchange between dark matter and dark energy. Similarly, the perturbation δ also tends towards zero for each model, suggesting a stabilization of the Hubble parameter perturbations over time. Additionally, the growth index γ exhibits a decreasing behavior as the universe expands, with its present value of $\gamma = 0.55$ being close to the ΛCDM prediction, implying a similar growth behavior at the current epoch. The growth rate f is also found to tend towards zero at late times, reinforcing the idea of a diminishing growth of matter perturbations in the distant future. Furthermore, we plotted the $f\sigma_8$ parameter as a function of redshift and found that the model predictions show good agreement with observational data, further supporting the viability of the BADE and NBADE models. These findings provide deeper insights into the dynamics of dark energy and suggest that the interaction between dark sectors could play a significant role in the evolution of large-scale structures in the universe.
- Thoroughly testing, improving, and confirming the Barrow agegraphic and new Barrow agegraphic dark energy models requires cosmographic study. It helps cosmologists determine if these theories are good options for explaining dark energy and the universe's accelerating expansion by bridging the gap between theoretical predictions and empirical data. Cosmographic research advances the larger objective of comprehending the basic nature of the universe by pointing out achievements and constraints. Cosmographic analysis evaluates the capability of BADE and NBADE models to characterize the expansion history of the universe and forecast future behavior by contrasting their predictions with high-precision cosmological observations (such as Type Ia supernovae, cosmic microwave background, and baryon acoustic oscillations).

Acknowledgements A. Kotal is thankful to IIEST, Shibpur, India for Institute Fellowship (JRF). A. Pradhan and U. Debnath express their sincere gratitude to the Inter-University Centre for Astronomy and Astrophysics (IUCAA), Pune, India, for providing research facilities under visiting Associateship program. The authors would like to thank the anonymous reviewer for their insightful criticism and recommendations, which have helped to make the paper better in its current state.

Data Availability Statement This manuscript has no associated data. [Authors' comment: As our study is grounded in theoretical analysis and mathematical modeling, it does not utilize any specific experimental or observational datasets. Consequently, there is no empirical data associated with this work, and data deposition is not applicable.]

Code Availability Statement This manuscript has no associated code/software. [Authors' comment: We employed Mathematica and Python for the numerical computations and graphical analyses presented in this study. No additional code or software was developed or utilized during the course of this research.]

Funded by SCOAP[3].

References

1. A.G. Cohen, D.B. Kaplan, A.E. Nelson, Effective field theory, black holes, and the cosmological constant. Phys. Rev. Lett. **82**(25), 4971–4974 (1999). https://doi.org/10.1103/physrevlett.82.4971
2. M. Li, A model of holographic dark energy. Phys. Lett. B **603**(1–2), 1–5 (2004). https://doi.org/10.1016/j.physletb.2004.10.014
3. S. Wang, Y. Wang, M. Li, Holographic dark energy. Phys. Rep. **696**, 1–57 (2017). https://doi.org/10.1016/j.physrep.2017.06.003
4. R.-G. Cai, A dark energy model characterized by the age of the universe. Phys. Lett. B **657**(4–5), 228–231 (2007). https://doi.org/10.1016/j.physletb.2007.09.061
5. R.-G. Cai, A dark energy model characterized by the age of the universe. Phys. Lett. B **657**, 228–231 (2007). https://doi.org/10.1016/j.physletb.2007.09.061. arXiv:0707.4049
6. Y. Zhang, H. Li, X. Wu, H. Wei, R.-G. Cai, Age constraints on the agegraphic dark energy model (2007). arXiv:0708.1214
7. H. Wei, R.-G. Cai, A new model of agegraphic dark energy. Phys. Lett. B **660**(3), 113–117 (2008). https://doi.org/10.1016/j.physletb.2007.12.030
8. K.Y. Kim, H.W. Lee, Y.S. Myung, Instability of agegraphic dark energy models. Phys. Lett. B **660**, 118–124 (2008). https://doi.org/10.1016/j.physletb.2007.12.045. arXiv:0709.2743
9. Y. Li, J. Ma, J. Cui, Z. Wang, X. Zhang, Interacting model of new agegraphic dark energy: observational constraints and age problem. Sci. China Phys. Mech. Astron. **54**, 1367–1377 (2011). https://doi.org/10.1007/s11433-011-4382-1. arXiv:1011.6122
10. X. Wu, Y. Zhang, H. Li, R.-G. Cai, Z.-H. Zhu, Observational constraints on agegraphic dark energy (2007). arXiv:0708.0349
11. H. Wei, R.-G. Cai, Cosmological constraints on new agegraphic dark energy. Phys. Lett. B **663**, 1–6 (2008). https://doi.org/10.1016/j.physletb.2008.03.048. arXiv:0708.1894
12. M.A. Zadeh, A. Sheykhi, H. Moradpour, Tsallis agegraphic dark energy model. Mod. Phys. Lett. A **34**(11), 1950086 (2019). https://doi.org/10.1142/s021773231950086x
13. Pankaj, B.D. Pandey, P.S. Kumar, U.K. Sharma, New Tsallis agegraphic dark energy. Int. J. Mod. Phys. D **31**(13) (2022). https://doi.org/10.1142/s0218271822501024
14. J.D. Barrow, The area of a rough black hole. Phys. Lett. B **808**, 135643 (2020). https://doi.org/10.1016/j.physletb.2020.135643
15. U.K. Sharma, G. Varshney, V.C. Dubey, Barrow agegraphic dark energy. Int. J. Mod. Phys. D **30**(03), 2150021 (2021). https://doi.org/10.1142/S0218271821500218
16. E.N. Saridakis, Barrow holographic dark energy. Phys. Rev. D **102**, 123525 (2020). https://doi.org/10.1103/PhysRevD.102.123525
17. J.D. Barrow, The area of a rough black hole. Phys. Lett. B **808**, 135643 (2020). https://doi.org/10.1016/j.physletb.2020.135643. arXiv:2004.09444
18. E.N. Saridakis, Barrow holographic dark energy. Phys. Rev. D **102**, 123525 (2020). https://doi.org/10.1103/PhysRevD.102.123525
19. F.K. Anagnostopoulos, S. Basilakos, E.N. Saridakis, Observational constraints on barrow holographic dark energy. Eur. Phys. J. C **80**(9), 826 (2020). https://doi.org/10.1140/epjc/s10052-020-8360-5. arXiv:2005.10302
20. A.A. Mamon, A. Paliathanasis, S. Saha, Dynamics of an interacting barrow holographic dark energy model and its thermodynamic implications. Eur. Phys. J. Plus **136**(1), 134 (2021). https://doi.org/10.1140/epjp/s13360-021-01130-7. arXiv:2007.16020
21. C. Tsallis, Possible generalization of Boltzmann–Gibbs statistics. J. Stat. Phys. **52**, 479–487 (1988). https://doi.org/10.1007/BF01016429
22. C. Tsallis, L. Cirto, Black hole thermodynamical entropy. Eur. Phys. J. C **73**, 2487 (2013). https://doi.org/10.1140/epjc/s10052-013-2487-6. arXiv:1202.2154
23. G. Wilk, Z. Wlodarczyk, On the interpretation of nonextensive parameter q in Tsallis statistics and Levy distributions. Phys. Rev. Lett. **84**, 2770 (2000). https://doi.org/10.1103/PhysRevLett.84.2770. arXiv:hep-ph/9908459
24. E.N. Saridakis, Modified cosmology through spacetime thermodynamics and barrow horizon entropy. J. Cosmol. Astropart. Phys. **2020**(07), 031031 (2020). https://doi.org/10.1088/1475-7516/2020/07/031
25. S. Maity, P. Rudra, Inflation driven by Barrow holographic dark energy. JHAP **2**(1), 1–12 (2022). https://doi.org/10.22128/jhap.2022.464.1012. arXiv:2202.08160
26. R.A. Pankaj, U.K. Sharma, N.M. Ali, Cosmological evolution and stability analysis in non-flat universe and Barrow holographic model of dark energy. Astrophys. Space Sci. **368**(3), 15 (2023). https://doi.org/10.1007/s10509-023-04174-6
27. A. Kumar, V. Srivastava, V.C. Dubey, U.K. Sharma, Statefinder diagnosis for Barrow agegraphic dark energy. Int. J. Geom. Methods Mod. Phys. **20**(07), 2350112 (2023). https://doi.org/10.1142/S0219887823501128
28. N. Boulkaboul, Baryogenesis triggered by Barrow holographic dark energy coupling. Phys. Dark Univ. **40**, 101205 (2023). https://doi.org/10.1016/j.dark.2023.101205
29. U.K. Sharma, G. Varshney, V.C. Dubey, Barrow agegraphic dark energy. Int. J. Mod. Phys. D **30**(03), 2150021 (2021). https://doi.org/10.1142/s0218271821500218
30. H. Huang, Q. Huang, R. Zhang, Phase space analysis of Barrow agegraphic dark energy. Universe **8**(9), 467 (2022). https://doi.org/10.3390/universe8090467
31. M. Kumar, U.K. Sharma, V.C. Dubey, Analysis of new barrow agegraphic dark energy with different diagnostic tools. Int. J. Geom. Methods Mod. Phys. **20**(03), 2350043 (2023). https://doi.org/10.1142/S0219887823500433
32. G.G. Luciano, Cosmic evolution and thermal stability of barrow holographic dark energy in a nonflat Friedmann–Robertson–Walker universe. Phys. Rev. D **106**, 083530 (2022). https://doi.org/10.1103/PhysRevD.106.083530
33. P. Adhikary, S. Das, S. Basilakos, E.N. Saridakis, Barrow holographic dark energy in a nonflat universe. Phys. Rev. D **104**(12), 123519 (2021). https://doi.org/10.1103/PhysRevD.104.123519. arXiv:2104.13118
34. Pankaj, B.D. Pandey, P.S. Kumar, U.K. Sharma, New Tsallis agegraphic dark energy. Int. J. Mod. Phys. D **31**(13), 2250102 (2022). https://doi.org/10.1142/S0218271822501024. arXiv:2205.01095
35. M. Mahmoudifard, A. Salehi, R. Sepahvand, Constraining neutrino masses in the Barrow holographic dark energy model with Granda-Oliveros IR cutoff. Eur. Phys. J. C **84**(10), 1099 (2024). https://doi.org/10.1140/epjc/s10052-024-13466-2
36. B. Chakraborty, T. Mukhopadhyay, A. Kotal, U. Debnath, Reconstructions of Einstein–Aether gravity from barrow agegraphic and new barrow agegraphic dark energy models: examinations and observational limits (2024). arXiv:2410.19897
37. T. Mukhopadhyay, B. Chakraborty, A. Kotal, U. Debnath, Reconstructions of $f(\mathcal{P})$ and $f(\mathcal{Q})$ gravity models from (m, n)-type Barrow holographic dark energy: analysis and observational constraints (2024). https://doi.org/10.1142/S0219887825500513. arXiv:2405.08050
38. A. Pradhan, V.K. Bhardwaj, P. Garg, S. Krishnannair, FRW cosmological models with Barrow holographic dark energy in Brans–Dicke theory. Int. J. Geom. Methods Mod. Phys. **19**(07), 2250106 (2022). https://doi.org/10.1142/S0219887822501067
39. P. Garg, V.K. Bhardwaj, A. Pradhan, Barrow entropic quintessence and dilation dark energy models with generalized

HDE cut-off. Int. J. Mod. Phys. A **37**(36), 2250217 (2022). https://doi.org/10.1142/S0217751X22502177. arXiv:2303.10376
40. P. Garg, A. Pradhan, V.K. Bhardwaj, Generalized Barrow entropic holographic dark energy with Granda-Oliver cut-off. Int. J. Geom. Methods Mod. Phys. **20**(05), 2350082 (2023). https://doi.org/10.1142/S0219887823500822
41. G.G. Luciano, Constraining barrow entropy-based cosmology with power-law inflation. Eur. Phys. J. C **83**(4), 1434–6052 (2023). https://doi.org/10.1140/epjc/s10052-023-11499-7
42. A. Khodam-Mohammadi, Non-extensive entropy and power-law inflation: implications for observations. Mod. Phys. Lett. A **39**(31n32), 2450146 (2024). https://doi.org/10.1142/S0217732324501463
43. T. Clemson, K. Koyama, G.-B. Zhao, R. Maartens, J. Valiviita, Interacting dark energy—constraints and degeneracies. Phys. Rev. D **85**, 043007 (2012). https://doi.org/10.1103/PhysRevD.85.043007. arXiv:1109.6234,
44. T. Koivisto et al., Formation of structure in dark energy cosmologies. Helsinki Institute of Physics, Internal report series (2006)
45. G. Ellis, R. Maartens, The emergent universe: inflationary cosmology with no singularity. Class. Quantum Gravity **21**, 223–232 (2004). https://doi.org/10.1088/0264-9381/21/1/015. arXiv:gr-qc/0211082
46. C.B. Netterfield et al., A measurement by Boomerang of multiple peaks in the angular power spectrum of the cosmic microwave background. Astrophys. J. **571**, 604–614 (2002). https://doi.org/10.1086/340118. arXiv:astro-ph/0104460
47. J.L. Sievers et al., Cosmological parameters from Cosmic Background Imager observations and comparisons with BOOMERANG, DASI, and MAXIMA. Astrophys. J. **591**, 599–622 (2003). https://doi.org/10.1086/375510. arXiv:astro-ph/0205387
48. A. Benoit et al., The cosmic microwave background anisotropy power spectrum measured by Archeops. Astron. Astrophys. **399**, L19–L23 (2003). https://doi.org/10.1051/0004-6361:20021850. arXiv:astro-ph/0210305
49. A. Benoit et al., Cosmological constraints from Archeops. Astron. Astrophys. **399**, L25–L30 (2003). https://doi.org/10.1051/0004-6361:20021722. arXiv:astro-ph/0210306
50. G. Efstathiou, Is the low CMB quadrupole a signature of spatial curvature? Mon. Not. R. Astron. Soc. **343**, L95 (2003). https://doi.org/10.1046/j.1365-8711.2003.06940.x. arXiv:astro-ph/0303127
51. J.-P. Uzan, U. Kirchner, G. Ellis, WMAP data and the curvature of space. Mon. Not. R. Astron. Soc. **344**, L65 (2003). https://doi.org/10.1046/j.1365-8711.2003.07043.x. arXiv:astro-ph/0302597
52. A.D. Linde, Can we have inflation with Omega > 1? JCAP **05**, 002 (2003). https://doi.org/10.1088/1475-7516/2003/05/002. arXiv:astro-ph/0303245
53. R.R. Caldwell, M. Kamionkowski, Expansion, geometry, and gravity. JCAP **09**, 009 (2004). https://doi.org/10.1088/1475-7516/2004/09/009. arXiv:astro-ph/0403003
54. B. Wang, Y.-G. Gong, R.-K. Su, Probing the curvature of the universe from supernova measurement. Phys. Lett. B **605**, 9–14 (2005). https://doi.org/10.1016/j.physletb.2004.11.027. arXiv:hep-th/0408032
55. K.R. Mishra, S. Pacif, R. Kumar, K. Bamba, Cosmological implications of an interacting model of dark matter & dark energy. Phys. Dark Univ. **40**, 101211 (2023). https://doi.org/10.1016/j.dark.2023.101211. arXiv:2301.08743
56. U.K. Sharma, M. Kumar, Barrow holographic phantom. Int. J. Geom. Methods Mod. Phys. **19**(05), 2250066 (2022). https://doi.org/10.1142/S0219887822500669
57. Y.L. Bolotin, A. Kostenko, O.A. Lemets, D.A. Yerokhin, Cosmological evolution with interaction between dark energy and dark matter. Int. J. Mod. Phys. D **24**(03), 1530007 (2014). https://doi.org/10.1142/S0218271815300074. arXiv:1310.0085
58. B. Wang, J. Zang, C.-Y. Lin, E. Abdalla, S. Micheletti, Interacting dark energy and dark matter: observational constraints from cosmological parameters. Nucl. Phys. B **778**, 69–84 (2007). https://doi.org/10.1016/j.nuclphysb.2007.04.037. arXiv:astro-ph/0607126
59. H. Moradpour, R.C. Nunes, E.M.C. Abreu, J.A. Neto, A note on the relations between thermodynamics, energy definitions and Friedmann equations. Mod. Phys. Lett. A **32**(13) (2017). https://doi.org/10.1142/S021773231750078X. arXiv:1603.01465
60. F.C. Santos, M.L. Bedran, V. Soares, On the thermodynamic stability of the generalized Chaplygin gas. Phys. Lett. B **636**, 86–90 (2006). https://doi.org/10.1016/j.physletb.2006.03.042
61. E.M. Barboza, R.C. Nunes, E. Abreu, J.A. Neto, Thermodynamic aspects of dark energy fluids. Phys. Rev. D **92**(8), 083526 (2015). https://doi.org/10.1103/PhysRevD.92.083526. arXiv:1501.03491
62. P. Bhandari, S. Haldar, S. Chakraborty, Interacting dark energy model and thermal stability. Eur. Phys. J. C **77**(12), 840 (2017). https://doi.org/10.1140/epjc/s10052-017-5417-1
63. M. Abdollahi Zadeh, A. Sheykhi, H. Moradpour, Thermal stability of Tsallis holographic dark energy in nonflat universe. Gen. Relativ. Gravit. **51**(1), 12 (2019). https://doi.org/10.1007/s10714-018-2497-7
64. G.G. Luciano, Cosmic evolution and thermal stability of Barrow holographic dark energy in a nonflat Friedmann–Robertson–Walker Universe. Phys. Rev. D **106**(8), 083530 (2022). https://doi.org/10.1103/PhysRevD.106.083530. arXiv:2210.06320
65. H. Ooguri, C. Vafa, On the geometry of the string landscape and the swampland. Nucl. Phys. B **766**, 21–33 (2007). https://doi.org/10.1016/j.nuclphysb.2006.10.033. arXiv:hep-th/0605264
66. A. Dixit, A. Pradhan, Stability, dark energy parameterization and swampland aspect of Bianchi type-VI_h cosmological models with $f(R,T)$-gravity. Int. J. Geom. Methods Mod. Phys. **17**(14), 2050213 (2020). https://doi.org/10.1142/S0219887820502138. arXiv:2003.14242
67. M. Benetti, S. Capozziello, L.L. Graef, Swampland conjecture in $f(R)$ gravity by the Noether symmetry approach. Phys. Rev. D **100**(8), 084013 (2019). https://doi.org/10.1103/PhysRevD.100.084013. arXiv:1905.05654
68. M.C. David Marsh, The swampland, quintessence and the vacuum energy. Phys. Lett. B **789**, 639–642 (2019). https://doi.org/10.1016/j.physletb.2018.11.001. arXiv:1809.00726
69. S. Brahma, M.W. Hossain, Dark energy beyond quintessence: constraints from the swampland. JHEP **06**, 070 (2019). https://doi.org/10.1007/JHEP06(2019)070. arXiv:1902.11014
70. K.R. Mishra, S.K.J. Pacif, R. Kumar, K. Bamba, Cosmological implications of an interacting dark energy model with the matter fields. arXiv-2301 (2023)
71. A. Lewis, S. Bridle, Cosmological parameters from CMB and other data: a Monte Carlo approach. Phys. Rev. D **66**, 103511 (2002). https://doi.org/10.1103/PhysRevD.66.103511. arXiv:astro-ph/0205436
72. G.S. Sharov, V.O. Vasiliev, How predictions of cosmological models depend on Hubble parameter data sets. Math. Model. Geom. **6**, 1–20 (2018). https://doi.org/10.26456/mmg/2018-611. arXiv:1807.07323
73. A. Gelman, J.B. Carlin, H.S. Stern, D.B. Rubin, *Bayesian Data Analysis* (Chapman and Hall/CRC, London, 1995)
74. M. Tegmark, A. Taylor, A. Heavens, Karhunen–Loeve eigenvalue problems in cosmology: how should we tackle large data sets? Astrophys. J. **480**, 22 (1997). https://doi.org/10.1086/303939. arXiv:astro-ph/9603021

75. H. Akaike, A new look at the statistical model identification. IEEE Trans. Autom. Control **19**(6), 716–723 (1974). https://doi.org/10.1109/TAC.1974.1100705
76. G. Schwarz, Estimating the dimension of a model. Ann. Stat. 461–464 (1978)
77. H. Jeffreys, *The Theory of Probability* (OuP, Oxford, 1998)
78. E. Gaztanaga, C. Bonvin, L. Hui, Measurement of the dipole in the cross-correlation function of galaxies. JCAP **01**, 032 (2017). https://doi.org/10.1088/1475-7516/2017/01/032. arXiv:1512.03918
79. J. Niu, T.-J. Zhang, Cosmological joint analysis with cosmic growth and expansion rate. Phys. Dark Univ. **39**, 101147 (2023). https://doi.org/10.1016/j.dark.2022.101147. arXiv:2204.10597
80. K. Jiao, N. Borghi, M. Moresco, T.-J. Zhang, New observational H(z) data from full-spectrum fitting of cosmic chronometers in the LEGA-C survey. Astrophys. J. Suppl. **265**(2), 48 (2023). https://doi.org/10.3847/1538-4365/acbc77. arXiv:2205.05701
81. C. Bengaly, M.A. Dantas, L. Casarini, J. Alcaniz, Measuring the Hubble constant with cosmic chronometers: a machine learning approach. Eur. Phys. J. C **83**(6), 548 (2023)
82. A.J. Ross, L. Samushia, C. Howlett, W.J. Percival, A. Burden, M. Manera, The clustering of the SDSS DR7 main Galaxy sample—I. A 4 per cent distance measure at $z = 0.15$. Mon. Not. R. Astron. Soc. **44**(1), 835–847 (2015). https://doi.org/10.1093/mnras/stv154. arXiv:1409.3242
83. S. Alam et al., The clustering of galaxies in the completed SDSS-III Baryon Oscillation Spectroscopic Survey: cosmological analysis of the DR12 galaxy sample. Mon. Not. R. Astron. Soc. **470**(3), 2617–2652 (2017). https://doi.org/10.1093/mnras/stx721. arXiv:1607.03155
84. H. Gil-Marin et al., The Completed SDSS-IV extended Baryon Oscillation Spectroscopic Survey: measurement of the BAO and growth rate of structure of the luminous red galaxy sample from the anisotropic power spectrum between redshifts 0.6 and 1.0. Mon. Not. R. Astron. Soc. **498**(2), 2492–2531 (2020). https://doi.org/10.1093/mnras/staa2455. arXiv:2007.08994
85. A. Raichoor et al., The completed SDSS-IV extended baryon oscillation spectroscopic survey: large-scale structure catalogues and measurement of the isotropic BAO between redshift 0.6 and 1.1 for the emission line galaxy sample. Mon. Not. R. Astron. Soc. **500**(3), 3254–3274 (2020). https://doi.org/10.1093/mnras/staa3336. arXiv:2007.09007
86. J. Hou et al., The Completed SDSS-IV extended baryon oscillation spectroscopic survey: BAO and RSD measurements from anisotropic clustering analysis of the Quasar Sample in configuration space between redshift 0.8 and 2.2. Mon. Not. R. Astron. Soc. **500**(1), 1201–1221 (2020). https://doi.org/10.1093/mnras/staa3234. arXiv:2007.08998
87. H. du Mas des Bourboux et al., The completed SDSS-IV extended baryon oscillation spectroscopic survey: baryon acoustic oscillations with Lyα forests. Astrophys. J. **901**(2), 153 (2020). https://doi.org/10.3847/1538-4357/abb085. arXiv:2007.08995
88. T. Abbott et al., Dark energy survey year 3 results: a 2.7% measurement of baryon acoustic oscillation distance scale at redshift 0.835. Phys. Rev. D **105**(4), 043512 (2022). https://doi.org/10.1103/PhysRevD.105.043512. arXiv:2107.04646
89. P. Collaboration, N. Aghanim, Y. Akrami, M. Ashdown, J. Aumont, C. Baccigalupi, M. Ballardini, A. Banday, R. Barreiro, N. Bartolo, et al., Planck 2018 results. vi. cosmological parameters (2020)
90. A.G. Riess, S. Casertano, W. Yuan, L.M. Macri, D. Scolnic, Large magellanic cloud cepheid standards provide a 1% foundation for the determination of the Hubble constant and stronger evidence for physics beyond ΛCDM. Astrophys. J. **876**(1), 85 (2019). https://doi.org/10.3847/1538-4357/ab1422. arXiv:1903.07603
91. K.P. Nandhida, T.K. Mathew, Barrow holographic dark energy model with GO cut-off—an alternative perspective. Int. J. Mod. Phys. D **31**, 2250107 (2022). https://doi.org/10.1142/S0218271822501073. arXiv:2112.07310
92. G.G. Luciano, E.N. Saridakis, Baryon asymmetry from Barrow entropy: theoretical predictions and observational constraints. Eur. Phys. J. C **82**(6), 558 (2022). https://doi.org/10.1140/epjc/s10052-022-10530-7. arXiv:2203.12010
93. J.D. Barrow, S. Basilakos, E.N. Saridakis, Big Bang Nucleosynthesis constraints on Barrow entropy. Phys. Lett. B **815**, 136134 (2021). https://doi.org/10.1016/j.physletb.2021.136134. arXiv:2010.00986
94. S. Di Gennaro, Y.C. Ong, Sign switching dark energy from a running barrow entropy. Universe **8**(10), 541 (2022). https://doi.org/10.3390/universe8100541. arXiv:2205.09311
95. A.A. Mamon, Constraints on a generalized deceleration parameter from cosmic chronometers. Mod. Phys. Lett. A **33**(10n11), 1850056 (2018). https://doi.org/10.1142/S0217732318500566. arXiv:1702.04916
96. Z. Li, P. Wu, H. Yu, Examining the cosmic acceleration with the latest Union2 supernova data. Phys. Lett. B **695**, 1–8 (2011). https://doi.org/10.1016/j.physletb.2010.10.044. arXiv:1011.1982
97. U. Alam, V. Sahni, T. Deep Saini, A. Starobinsky, Exploring the expanding universe and dark energy using the statefinder diagnostic. Mon. Not. R. Astron. Soc. **344**(4), 1057–1074 (2003)
98. V. Sahni, T.D. Saini, A.A. Starobinsky, U. Alam, Statefinder a new geometrical diagnostic of dark energy. J. Exp. Theor. Phys. Lett. **77**, 201–206 (2003)
99. V.K. Bhardwaj, A. Dixit, A. Pradhan, Statefinder hierarchy model for the Barrow holographic dark energy. New Astron. **88**, 101623 (2021). https://doi.org/10.1016/j.newast.2021.101623. arXiv:2102.09946
100. A. Pradhan, A. Dixit, V.K. Bhardwaj, Barrow HDE model for Statefinder diagnostic in FLRW Universe. Int. J. Mod. Phys. A **36**(04), 2150030 (2021). https://doi.org/10.1142/S0217751X21500305. arXiv:2101.00176
101. R.R. Caldwell, E.V. Linder, The limits of quintessence. Phys. Rev. Lett. **95**, 141301 (2005). https://doi.org/10.1103/PhysRevLett.95.141301. arXiv:astro-ph/0505494
102. R.J. Scherrer, Dark energy models in the w-w' plane. Phys. Rev. D **73**, 043502 (2006). https://doi.org/10.1103/PhysRevD.73.043502. arXiv:astro-ph/0509890
103. T. Chiba, W and w' of scalar field models of dark energy. Phys. Rev. D **73**, 063501 (2006). [Erratum: Phys. Rev. D **80**, 129901 (2009)]. https://doi.org/10.1103/PhysRevD.80.129901. arXiv:astro-ph/0510598
104. M. Koussour, S.H. Shekh, M. Bennai, Bianchi type-I Barrow holographic dark energy model in symmetric teleparallel gravity. Int. J. Mod. Phys. A **37**(28n29), 2250184 (2022). https://doi.org/10.1142/S0217751X22501846. arXiv:2203.08181
105. Y. Sobhanbabu, M. Vijaya Santhi, Kantowski–Sachs Tsallis holographic dark energy model with sign-changeable interaction. Eur. Phys. J. C **81**(11), 1040 (2021). https://doi.org/10.1140/epjc/s10052-021-09815-0
106. A.A. Mamon, P. Bhandari, S. Chakraborty, Study of thermal stability for different dark energy models. Int. J. Geom. Methods Mod. Phys. **16**(11), 11 (2019). https://doi.org/10.1142/S0219887819501718. arXiv:1802.07925
107. R.-G. Cai, S. Khimphun, B.-H. Lee, S. Sun, G. Tumurtushaa, Y.-L. Zhang, Emergent dark universe and the swampland criteria. Phys. Dark Univ. **26**, 100387 (2019). https://doi.org/10.1016/j.dark.2019.100387. arXiv:1812.11105
108. V.K. Oikonomou, Rescaled Einstein–Hilbert gravity from $f(R)$ gravity: inflation, dark energy and the swampland criteria.

Phys. Rev. D **103**(12), 124028 (2021). https://doi.org/10.1103/PhysRevD.103.124028. arXiv:2012.01312
109. R.M. Wald, *Quantum Field Theory in Curved Spacetime and Black Hole Thermodynamics* (University of Chicago Press, Chicago, 1994)
110. A. Bouali, H. Chaudhary, U. Debnath, A. Sardar, G. Mustafa, Data analysis of three parameter models of deceleration parameter in FLRW universe. Eur. Phys. J. Plus **138**(9), 816 (2023). https://doi.org/10.1140/epjp/s13360-023-04442-y. arXiv:2304.13137
111. J.K. Singh, R. Nagpal, A model of dark matter-dark energy interaction with some cosmic consequences. Indian J. Phys. **98**(7), 2609–2622 (2024). https://doi.org/10.1007/s12648-023-03002-5. arXiv:2311.13607
112. N.M. Garcia, T. Harko, F. Lobo, J.P. Mimoso, Energy conditions in modified Gauss–Bonnet gravity. Phys. Rev. D **83**, 104032 (2011). https://doi.org/10.1103/PhysRevD.83.104032. arXiv:1011.4159,
113. J.K. Singh, H. Balhara, K. Bamba, J. Jena, Bouncing cosmology in modified gravity with higher-order curvature terms. JHEP **03**, 191 (2023). [Erratum: JHEP **04**, 049 (2023)]. https://doi.org/10.1007/JHEP03(2023)191. arXiv:2206.12423
114. C. Barcelo, M. Visser, Twilight for the energy conditions? Int. J. Mod. Phys. D **11**, 1553–1560 (2002). https://doi.org/10.1142/S0218271802002888. arXiv:gr-qc/0205066
115. M. Visser, *Lorentzian Wormholes. From Einstein to Hawking* (Woodbury, New York, 1995)
116. A. Mussatayeva, N. Myrzakulov, M. Koussour, Cosmological constraints on dark energy in f(Q) gravity: a parametrized perspective. Phys. Dark Univ. **42**, 101276 (2023). https://doi.org/10.1016/j.dark.2023.101276. arXiv:2307.00281
117. L.-M. Wang, P.J. Steinhardt, Cluster abundance constraints on quintessence models. Astrophys. J. **508**, 483–490 (1998). https://doi.org/10.1086/306436. arXiv:astro-ph/9804015
118. W. Khyllep, A. Paliathanasis, J. Dutta, Cosmological solutions and growth index of matter perturbations in $f(Q)$ gravity. Phys. Rev. D **103**(10), 103521 (2021). https://doi.org/10.1103/PhysRevD.103.103521. arXiv:2103.08372
119. J. Dossett, M. Ishak, Effects of dark energy perturbations on cosmological tests of general relativity. Phys. Rev. D **88**(10), 103008 (2013). https://doi.org/10.1103/PhysRevD.88.103008. arXiv:1311.0726
120. L. Kazantzidis, L. Perivolaropoulos, Evolution of the $f\sigma_8$ tension with the Planck15/ΛCDM determination and implications for modified gravity theories. Phys. Rev. D **97**(10), 103503 (2018). https://doi.org/10.1103/PhysRevD.97.103503. arXiv:1803.01337
121. L.P. Chimento, D. Pavon, Dual interacting cosmologies and late accelerated expansion. Phys. Rev. D **73**, 063511 (2006). https://doi.org/10.1103/PhysRevD.73.063511. arXiv:gr-qc/0505096
122. L.P. Chimento, A.S. Jakubi, D. Pavon, W. Zimdahl, Interacting quintessence solution to the coincidence problem. Phys. Rev. D **67**, 083513 (2003). https://doi.org/10.1103/PhysRevD.67.083513. arXiv:astro-ph/0303145
123. W. Zimdahl, D. Pavon, Interacting quintessence. Phys. Lett. B **521**, 133–138 (2001). https://doi.org/10.1016/S0370-2693(01)01174-1. arXiv:astro-ph/0105479
124. G. Olivares, F. Atrio-Barandela, D. Pavon, Observational constraints on interacting quintessence models. Phys. Rev. D **71**, 063523 (2005). https://doi.org/10.1103/PhysRevD.71.063523. arXiv:astro-ph/0503242
125. G. Olivares, F. Atrio-Barandela, D. Pavon, Matter density perturbations in interacting quintessence models. Phys. Rev. D **74**, 043521 (2006). https://doi.org/10.1103/PhysRevD.74.043521. arXiv:astro-ph/0607604
126. A. Krolewski, S. Ferraro, M. White, Cosmological constraints from unWISE and Planck CMB lensing tomography. JCAP **12**(12), 028 (2021). https://doi.org/10.1088/1475-7516/2021/12/028. arXiv:2105.03421
127. C. Gruber, O. Luongo, Cosmographic analysis of the equation of state of the universe through Padé approximations. Phys. Rev. D **89**(10), 103506 (2014). https://doi.org/10.1103/PhysRevD.89.103506. arXiv:1309.3215
128. U. Alam, V. Sahni, A.A. Starobinsky, The case for dynamical dark energy revisited. JCAP **06**, 008 (2004). https://doi.org/10.1088/1475-7516/2004/06/008. arXiv:astro-ph/0403687
129. A.A. Mamon, K. Bamba, S. Das, Constraints on reconstructed dark energy model from SN Ia and BAO/CMB observations. Eur. Phys. J. C **77**(1), 29 (2017). https://doi.org/10.1140/epjc/s10052-016-4590-y. arXiv:1607.06631
130. J. Zheng, D.-C. Qiang, Z.-Q. You, Cosmological constraints on dark energy models using DESI BAO 2024 (2024). arXiv:2412.04830
131. T. Abbott et al., The dark energy survey: cosmology results with ∼1500 new high-redshift Type Ia Supernovae using the full 5 yr data set. Astrophys. J. Lett. **973**(1), L14 (2024). https://doi.org/10.3847/2041-8213/ad6f9f. arXiv:2401.02929
132. A.G. Adame et al., DESI 2024 VI: cosmological constraints from the measurements of baryon acoustic oscillations. JCAP **02**, 021 (2025). https://doi.org/10.1088/1475-7516/2025/02/021. arXiv:2404.03002
133. A.J. Shajib, J.A. Frieman, Evolving dark energy models: Current and forecast constraints (2025). arXiv:2502.06929
134. C.-G. Park, J. de Cruz Pérez, B. Ratra, Using non-DESI data to confirm and strengthen the DESI 2024 spatially flat w0waCDM cosmological parametrization result. Phys. Rev. D **110**(12), 123533 (2024). https://doi.org/10.1103/PhysRevD.110.123533. arXiv:2405.00502